The genomic response to drought across spatiotemporal scales in *Amaranthus tuberculatus*

Rozenn M. Pineau[1], Natalia Berchovich[2],
Loren H. Rieseberg[2], Julia M. Kreiner[1]

[1]Department of Ecology & Evolution, University of Chicago
[2]Department of Botany and Biodiversity Research Centre, University of British Columbia

Abstract

How genetic diversity responds to environmental change across spatiotemporal scales remains poorly understood despite its importance for species persistence in changing landscapes. Agricultural weeds offer ideal models for studying these adaptive dynamics as they rapidly evolve under both the intensive management practices designed to eliminate them and increasingly severe climate challenges such as drought. Here, we combine experimental and herbarium genomic approaches spanning within-generation to century-long timescales to understand how genome-wide variation responds to drought in *Amaranthus tuberculatus*. A history of divergent selection between two ancestral lineages is thought to play a role in this native species' invasion into agriculture. A drought survival experiment on accessions from paired agricultural and natural populations across its native range revealed substantial phenotypic variation differentiated by habitat, geography, and ancestry. Ancestry mapping revealed 43 independent regions across nearly all chromosomes that confer protective effects under drought, demonstrate particularly rapid allele frequency changes, and exhibit duration-specific selection over the course of the imposed drought. Observation of allele frequencies across the past century reveal evidence for climate-dependent fluctuating selection governing the evolution of drought-associated loci. Selection favors drought alleles during hot/dry years and selects against them in cool/wet years—a pattern more evident in long-term trends than in shorter temporal intervals, suggestive of adaptive lag in rapidly changing environments. By combining short and long-term spatiotemporal data, we demonstrate that fluctuating selection has preserved the polygenic variation underlying drought tolerance, enabling ongoing adaptive responses to contemporary land-use and climate change.

Introduction

Human activities are driving environmental change at unprecedented rates, creating intense and rapidly fluctuating selection pressures that challenge traditional evolutionary theory. The 'standard genetic model' assumes selection is weak, gradually depletes variation, and drives slow evolutionary change (1). This view, however, fails to capture the intensity and fluctuating nature of human land-use practices and climate change, which create spatially and temporally variable fitness landscapes across contemporary environments. When selection varies across space and time, fitness trade-offs mediate the balance between global evolutionary forces and local adaptive optima (2, 3). The rate at which populations adapt locally depends on the strength of selection relative to migration (4, 5) and the availability of adaptive genetic variation, with standing variation facilitating rapid responses (6). Understanding the implications of environmental change on adaptation and species persistence therefore requires quantifying how genetic variation responds to selection across relevant spatial and temporal scales.

While short-term responses can be measured across generations, they rarely predict long-term evolutionary dynamics (7–9). Temporal genomic field experiments have demonstrated that nonlinear and fluctuating selection can slow trait evolution while maintaining genetic variation (3, 10–12), and that climate-driven selection operates across seasonal to decadal timescales (12–15). The sequencing of historical herbarium samples spanning centuries of environmental change offer a powerful approach to address these phenomena in plant species (16–18), and has been leveraged to understand the consequences of changing land-use (19) and climate (20, 21). However, we still lack a clear understanding of how short-term adaptive responses under intense selection relate to longer-term evolutionary dynamics across contemporary landscapes (22, 23).

A particularly important adaptive response in plants occurs in response to drought, which imposes strong selective pressure through prolonged water limitation (24, 25) that varies dramatically in space, time, and intensity (26, 27). This spatial heterogeneity has long been recognized as important for plant ecotype formation (28, 29), with locally adapted types leveraging diverse physiological and ecological strategies ranging from altered phytohormone signaling (30, 31) to life history and resource allocation strategies (27). Given the complexity of strategies and traits involved, it is not surprising that drought tolerance is often polygenic (e.g. (32–34)). This architecture might further be expected to vary across populations due to locally varying optima (35), especially as adaptation to drought frequently imposes costs by reducing growth and reproduction (36, 37). Therefore, the extent and architecture of drought adaptation may differ considerably across environments with varying water availability, competition levels, and life history demands as is typical of contemporary landscapes, where human-mediated disturbance creates a mosaic of selection regimes.

Waterhemp (*Amaranthus tuberculatus*) is a species native to North America which has successfully expanded from wetland habitats into cultivated lands in the second half of the 20th century (38), presenting a powerful system for studying rapid adaptation (39, 40). Two

varieties within the species, var. *rudis* and var. *tuberculatus*, were historically isolated from one another by the Mississippi River but have been brought back into secondary contact (39, 41). Var. *rudis* ancestry has been favored during the species' invasion into cultivated lands (40), consistent with hypotheses that it was preadapted to agricultural habitats (39). Genomic time series from herbarium specimens have revealed how this ancestral standing genetic variation facilitated waterhemp's rapid response to agricultural intensification (19). However, we do not know what historical selective pressures maintained the genetic variation in var. *rudis* that enabled its success in agricultural environments (42). Given climatic differences across the species range, we hypothesized that higher exposure to drought in var. *rudis'* evolutionary history facilitated waterhemp's transition from riparian wetlands to drier agricultural landscapes.

Here, we test this hypothesis by characterizing variation in drought tolerance across *A. tuberculatus*' native range at both genomic and phenotypic scales. To do so, we first conducted a controlled drought survival experiment on range-wide accessions collected from paired agricultural and natural habitats, allowing us to disentangle the effects of geography, habitat type, and ancestry on drought tolerance. Using whole-genome sequencing of 280 individuals from this experiment, we employed admixture mapping to identify genomic regions underlying drought adaptation and tracked their allele frequency dynamics and phenotypic effects throughout an extended drought treatment. To understand the historical context of these adaptive loci, we analyzed climate-mediated selection patterns using herbarium specimens spanning over a century of environmental change, testing whether genomic regions important for drought survival today show signatures of past selection under variable climate conditions.

Results

Drought tolerance across the landscape varies by geography and environment

To understand how extreme bouts of selection vary in duration and frequency impact genomic and phenotypic variation across the landscape, we conducted a survival experiment. This experiment drew from accessions spanning 24 *Amaranthus tuberculatus* populations, where natural and agricultural habitats were collected pairwise across the Midwestern United States (12 pairs total, **Fig. 1A)** (40). After 3 weeks of growth (the 4-6 leaf stage), we stopped watering plants in the drought treatment (randomized full block design) and monitored survival by recording the day to full plant wilt (**Fig. S1**)–a proxy for survival under drought. In a mixed effects regression model of an individual's survival, controlling for block (bench, tray position effects) and size at imposed drought, we found significant individual level variation in drought tolerance by longitude ($F_{1,276} = 5.98$, p-value = 0.02).

Given our paired agricultural-natural sampling design, we further probed whether there were consistent differences in drought tolerance among populations depending on land-management—whether human-mediated agricultural or unmanaged natural lands. From population-specific survival curves, we determined the population drought-LD_{50}, defined as the number of days of drought exposure required to reach 50% mortality in the population (**Fig. 1B, Fig. S2**). Permuting habitat assignment among populations, we found that populations collected in agricultural habitats were significantly more resilient to drought as compared to those from natural habitats (permuted p-value = 0.004; **Fig. 1B-D**, **Fig. S3**). A multivariate regression of population LD_{50} supported this finding, with the least square mean LD_{50} in agricultural habitats equal to 11.4 days (SE = 0.37), as compared to 10.5 days (SE = 0.37) in natural habitats ($F_{3,20} = 3.85$, p-value = 0.03). Additionally, it recovered a longitudinal gradient in LD_{50} values, indicating better adaptation to water limitation in our most western populations (12.0 days, SE = 0.79) compared to easternmost populations (10.1 days, SE = 0.66) (**Fig. 1C**, longitude partial $R^2 = 0.06$ with a significant overall effect ($F_{1,22} = 7.49$, p-value = 0.01), consistent with repeated population responses to drought at geographic and environmental scales.

Ecological trade-offs often constrain species' responses to environmental stress (24), though rapid growth can enable drought escape by allowing development before severe water stress occurs. Herbicide resistance mechanisms like EPSPS gene amplification in response to glyphosate can impose growth costs (43), but their effects on drought tolerance remain unexplored. We investigated the relationship between growth, drought tolerance, and herbicide resistance using early growth rate measurements from the survival experiment and genomic estimates of EPSPS copy number (see *methods*). Individuals varied considerably in EPSPS copy number, with 61.5% showing no amplification and 38.5% showing amplification, up to 5.51 copies. Individual-level correlations suggested positive relationships between drought tolerance and both growth rate ($r^2 = 0.11$, p-value = 5.5×10^{-7}, **Fig. 1E**) and drought tolerance and herbicide resistance ($r^2 = 0.025$, p-value = 0.009, **Fig. S4**), potentially supporting drought escape, but contradicting expectations for tradeoffs of abiotic stress

tolerances. However, these relationships disappeared in multivariate models accounting for geography and habitat (**Fig. S5**). At the population level, agricultural populations consistently showed increased drought tolerance (**Fig. 1D;** Wilcoxon signed rank exact p-value = 0.05), higher frequencies of herbicide resistance (**Fig. S4C;** Wilcoxon signed rank exact p-value = 0.0002), and slower early growth rates compared to natural populations (**Fig. 1E;** Wilcoxon signed rank exact p-value = 6.80×10^{-7})– in contrast with individual level trait correlations. This scale-dependent pattern suggests correlated, habitat-dependent selective pressures overpower any individual level variation that would potentially support the evolution of drought escape strategies or physiological trade-offs.

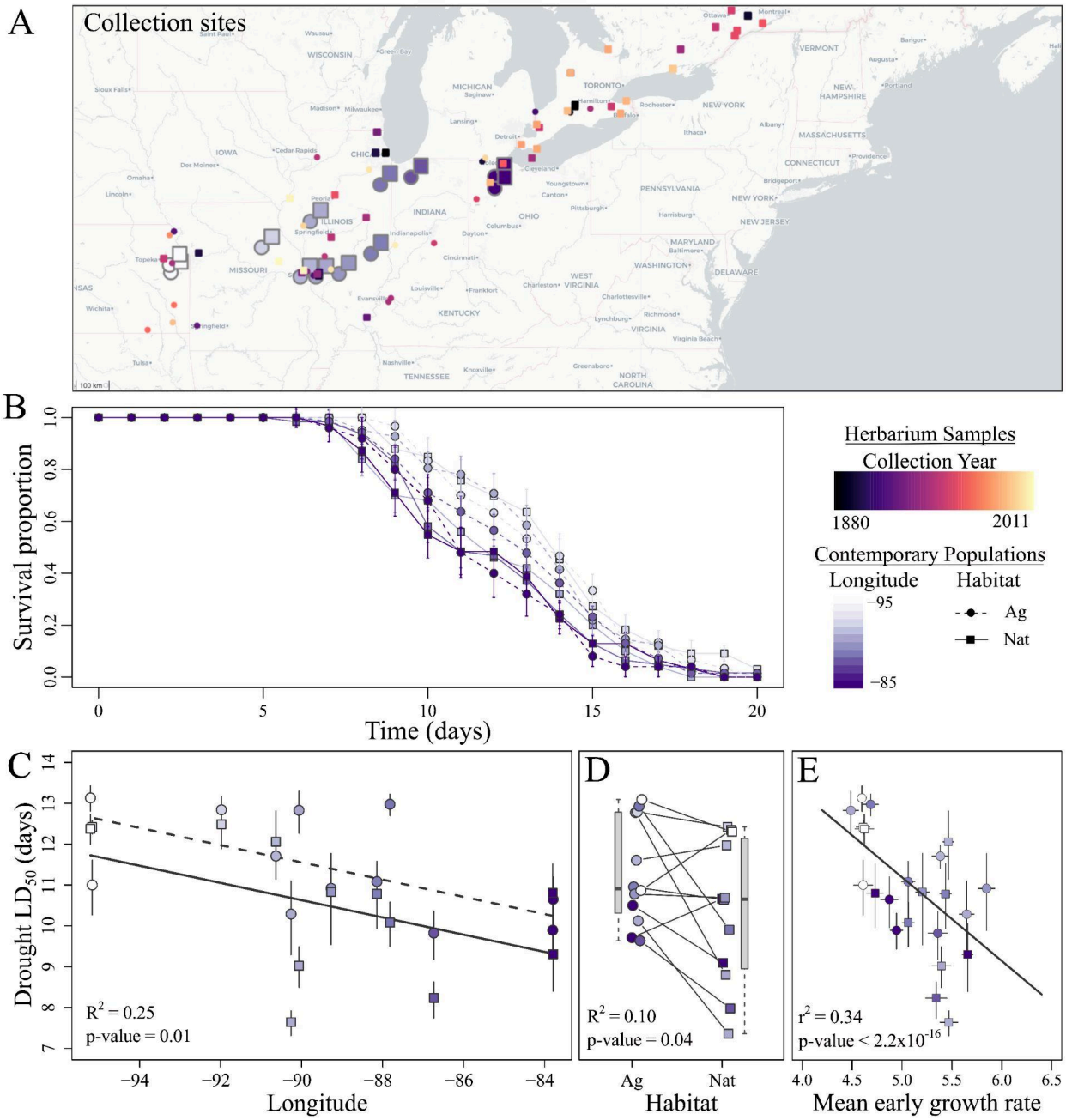

Fig. 1. Drought tolerance varies by habitat and across the geographic range of A. *tuberculatus*. (A) Paired agricultural and natural populations were collected on a southwestern to northeastern gradient, on both sides of the Mississippi river– spanning the ancestral ranges of *var. rudis* and *var. tuberculatus*. Samples are colored by longitude and environment is indicated by point type (see legend). Smaller circles denote the sequenced herbarium specimens' sampling location (from Kreiner et al., 2022), colored by collection year ranging from 1880 to 2011. (B) Plants from contemporary collections were subjected to a drought selection experiment and their survival over time was recorded. Points and lines represent means grouped by longitude and environment (legend as in A), error bars represent the standard error. (C) The drought LD_{50} (days until 50% mortality in a population) increases from east to west. (D) Populations collected from agricultural fields survive longer under drought as compared to samples collected from nearby natural areas. (E) Populations with longer survival under drought also have slower early growth rate (as measured in the control treatment under normal watering regimes; univariate linear regression).

Ancestry predicts response to drought

To understand how drought shapes genome-wide variation, we resequenced and analyzed whole-genomes from 280 individuals subjected to drought in our survival experiment. We found strong signatures of population structure consistent with previous work (19, 40). The first and second principal components (PC) of an ordination on genome-wide genotypes explains 17% and 6% of the variation among samples, and are strongly predicted by several geographic and environmental variables (*PC1 predictors*: latitude $F_{3, 276} = -8.94$, p-value $< 2 \times 10^{-16}$; longitude $F_{3, 276} = -9.83$, p-value $< 2 \times 10^{-16}$; and environment $F_{3, 276} = -4.37$, p-value $= 1.8 \times 10^{-5}$; *PC2 predictor*: environment $F_{3, 276} = -4.12$, p-value $= 5 \times 10^{-5}$, **Fig. 2A**). An ADMIXTURE analysis (44) with two ancestral populations (K=2) is best supported and collinear with PC1. Southwestern populations are dominated by one ancestry group and northeastern populations by another, consistent with the described distribution of *A. tuberculatus* var. *rudis* and var. *tuberculatus*, respectively (**Fig. 2A**).

We hypothesized that geographic and habitat-based patterns in drought tolerance may be explained by variation in ancestry composition. Indeed, we find that *var. rudis* ancestry provides a significant protective effect against drought in a multivariate regression regardless of whether we use an ADMIXTURE or PC based ancestry metric (**Table S1)**. This occurs both through a main effect and through ancestry's interaction with longitude (**Fig. 2C**, ancestry: $F_{1,16} = 5.96$, p-value = 0.03; longitude x ancestry: $F_{1,16} = 7.15$, p-value = 0.017, ancestry partial $R^2 = 0.31$. The longitude × ancestry interaction reveals that longitude predicts variation in drought LD_{50} among populations when var. *rudis* ancestry is rare or absent, but has no effect when var. *rudis* ancestry dominates (**Fig. S6)**. Near the centre of the range where ancestry varies considerably (-88° to -91°), a shift from pure var. *tuberculatus* to pure var. *rudis* results in 1.7-2.3 fold increase in LD_{50}. These results support that divergent evolutionary histories between lineages have produced substantial heritable variation in drought tolerance, providing a foundation for mapping the genomic architecture of drought.

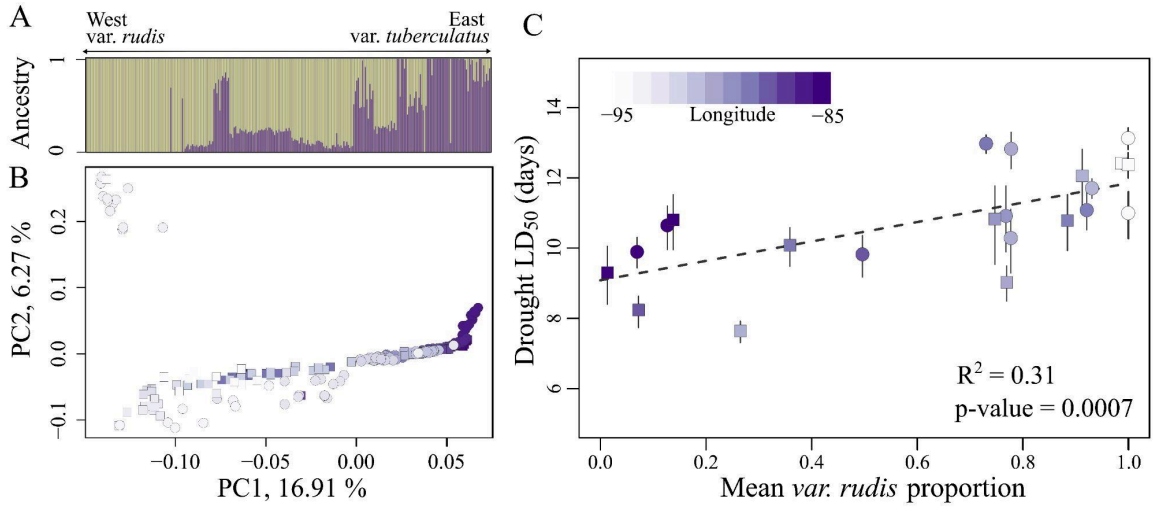

Fig. 2. Genome-wide ancestry predicts the response to drought. (A) Model based global ancestry inference (ADMIXTURE) demonstrates that our experiment spans a range of individual-level ancestry composition, with a gradient of ancestry going from pure var. *rudis* in the west to pure var. *tuberculatus* in the east. Samples are ordered by longitude. (B) Population structure as inferred by principal component (PC) analysis, with the first PC being collinear with longitude, such as we observe for ancestry. (B) The mean proportion of var. *rudis* ancestry in a population significantly predicts survival under drought (drought LD_{50}). Samples are colored by longitude in B&C.

Resolving the genetic architecture of drought tolerance

Given the strong association between var. *rudis* ancestry and drought tolerance in our system, we leveraged an admixture mapping approach to identify genomic regions underlying adaptation to water limitation. We performed local ancestry inference on our 280 resequenced samples using ancestry_hmm (see *methods*) (45) (**Fig. 3A**), leveraging 786,262 ancestry informative variants (~1.2 per kb) to call fine-scale ancestry across the genome. Under a two-pulse admixture model, our data is consistent with a first pulse of admixture 10,000 generations ago that introduced 0.42 proportion of var. *rudis* ancestry into var. *tuberculatus*, and a second pulse 7.4 generations ago which introduced 0.24 proportion of var. *rudis* ancestry. This fine-scale inference was highly concordant with estimates of genome-wide level ancestry inference, reinforcing the considerable variation in ancestry across individuals (**Fig. S7**).

We identified 893 significant associations between local ancestry and drought tolerance after FDR and genomic inflation factor correction ($q < 0.05$, $\lambda = 2.35$) while controlling for population structure using the kinship matrix (see *methods*; **Fig. 3A**). These drought associated loci are found across 13/16 chromosomes, with significant loci especially concentrated on chromosomes 5 (n=121), 6 (n=93) and 16 (n=433). Many of these loci fall within genes previously identified to have drought-relevant functions, including *HAT14* (β = 1.17 & p-value of lead locus = $9x10^{-7}$)(46), *APSR1* (β = 1.30 & p-value of lead locus = 0.0002) (47), *PER17* (β = 1.24 & p-value of lead locus = 0.02) (48) and *RKD5* (β = 1.27 & p-value of lead locus = 0.0006) (49), *TDC2* (β = 1.14 & p-value of lead locus = 0.001) (50),

and *DDB1* (β = 1.40 & p-value of lead locus = 5 x 10^{-5}) (51–53) (see full list in **Table S2**). GO biological processes for these drought-associated loci include terms such as mRNA processing (cleavage and splicing), plant growth (gravitropism, photomorphogenesis, root and leaf development), protein synthesis (tRNA), and ion metabolism (ion binding and transport) **(Table S3)**. An LD-informed clumping analysis of significant loci (see *methods*) identified 43 independent drought-associated regions across the genome, suggesting that drought tolerance is highly polygenic.

We next tested whether drought associated alleles were enriched in their differentiation among natural and agricultural habitats. Leveraging our paired sampling design, we implemented a Cochran-Mantel-Haenszel (CMH) scan to identify genomic regions involved in agricultural adaptation (as in 19), identifying 13,602 SNPs across the genome surpassing FDR correction (α=0.015, see *methods*, **Fig. S8**). Intersecting these putatively agriculturally-adaptive alleles with our drought-associated loci, we find that ~4% (35/893) of drought-associated loci are divergently selected among natural and agricultural habitats (**Fig. S8B**, falling in the genes *HAT14*, *RKD5*, *TBR*, *TDC2*). In a multivariate regression of ancestry composition at drought loci, we find that habitat significantly predicts the prevalence of protective loci after controlling for genome-wide ancestry composition, both through a main effect ($F_{1,271}$=4.34, p-value = 0.038) and its interactions with latitude ($F_{1,271}$=4.45, p-value = 0.036) and longitude ($F_{1,271}$=4.61, p-value = 0.033), with agricultural populations showing higher predicted frequencies of drought tolerance alleles than natural populations, especially in our most western (Δp Ag-Nat = 0.062) and northern populations (Δp Ag-Nat =0.088) (**Figs. S9, S10**). This suggests that pathways involved in adaptation to drought have also played a key role in shaping the invasion of waterhemp into agriculture.

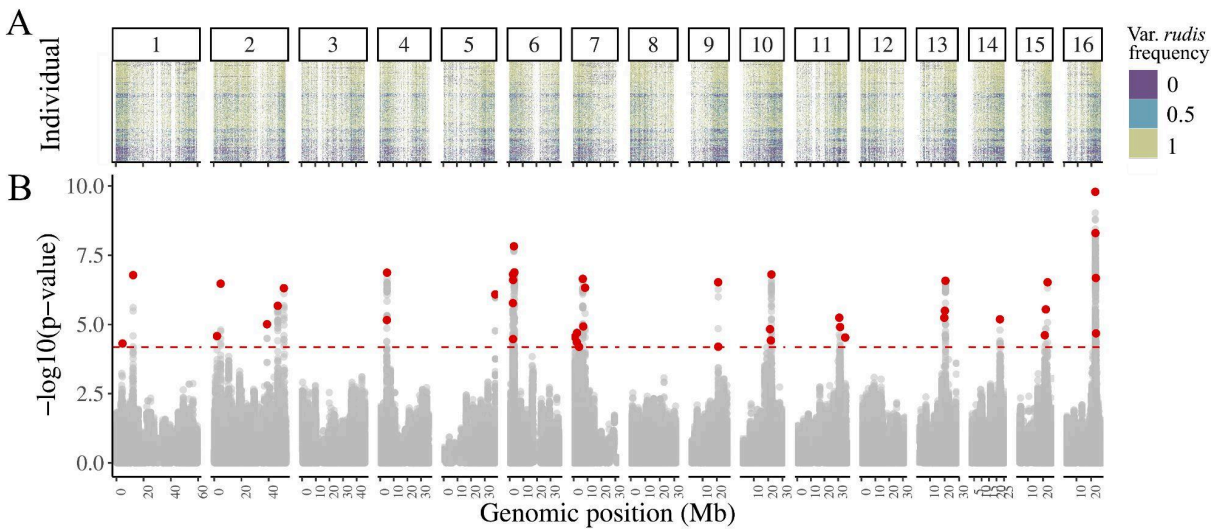

Fig. 3. Admixture mapping reveals the polygenic architecture underlying drought tolerance. (A) Fine-scale ancestry calls for 786,261 loci across the genome resulting from a two-pulse admixture model, with individuals ordered by longitude along the y axis (bottom to top, western to eastern). (B) Admixture mapping of survival under drought reveals 893 significantly associated loci after FDR and genomic inflation factor correction (q <0.05, λ = 2.35, lower dashed horizontal line), where red dots indicated focal index loci after LD clumping sites with r^2 > 0.50 within a 100 kb region.

The tempo of selective responses across an extreme drought event

Our drought survival experiment provides insight into the rate and scale of genomic response to selection imposed by extreme climate events. By tracking the 43 independent drought-associated loci over the progression of the imposed drought, we capture the selected allele frequency trajectories contributing to drought adaptation in *A. tuberculatus*. We find that the frequency of var. *rudis* haplotypes at all 43 drought-associated regions increase over the course of the selection experiment (**Fig. 4A-B**), providing further evidence for the protective effect of var. *rudis* ancestry under water limitation. This ancestry-specific response emerged despite a high background frequency of var. *rudis* (mean var. *rudis* frequency at the start of the experiment ~0.73) in our experimental design. To further distinguish selection at these sites from shifts in the genome-wide background, we contrasted the mean change in the frequency of these 43 drought-adapted loci against permutations of 43 randomly selected sites with a matching starting allele frequency distribution. We found an excess of change in drought-associated loci relative to these frequency-matched distributions (Z score = 1.47, p-value = 0.05; **Fig. 4B**), consistent with particularly strong selection imposed on these alleles in our experiment.

These time-series data revealed the strength of fitness advantages conferred by drought-alleles in our experiment. The within-generation survival-based selection coefficients (s_β) calculated through logistic regression of allele frequencies through time averaged 0.12 [SE = 0.012] and ranged from 0.097 to 0.14 (see *methods*), indicating strong selection favoring drought-tolerance alleles during the experimental drought event (**Fig. 4C**). If we consider how the length of such drought events mediate these responses, we observe a threshold response—where s_β intensified significantly between days 10 and 15 (twofold increase), before stabilizing after day 15 (**Fig. 4A**, top panel). This pattern suggests that drought adaptation involves a non-linear response to water limitation, with selection pressure accelerating dramatically between days 10-15 as plants exceed physiological tolerance thresholds, followed by a stabilization phase after day 15 when surviving individuals become enriched for drought-adaptive alleles.

To quantify the individual and joint contribution of drought-associated loci on individual-level variation in survival under drought, we implemented Cox proportional hazards tests. We calculated the polygenic score (PGS) for all 43 drought-associated loci to quantify their cumulative protective effects ($PGS = \Sigma[\beta_i \times A_i]$ (54), where β_i represents the effect size from GWAS for locus i and A_i represents the var. *rudis* ancestry dosage at that locus). With effect sizes ranging from 1.14 to 1.60 across these loci, polygenic scores varied from 0.65 to 56.67. Controlling for ancestry, this polygenic score significantly enhanced survival (hazard ratio = 0.87, p-value $< 2\times10^{-16}$), with each 10% increase in the PGS reducing mortality risk by 46%. Across the full range of observed scores, our model predicts a 500-fold difference in mortality risk between the most drought-tolerant and most susceptible individuals, highlighting the dramatic fitness consequences of variation at these loci. In this model, genome-wide var. *rudis* ancestry retains a significant predictive effect on drought

tolerance (hazard ratio = 0.0056, p-value = 7.64×10^{-13}), with each 10% increase in ancestry proportion reducing risk by 40%, consistent with additional drought-tolerance variants segregating beyond those detected in our GWAS. Individual locus effects revealed substantial variation in effect size of drought-protective loci, with hazard ratios spanning 0.51 to 0.91 among the 24 significant loci with significant effects in the multivariate cox hazard model (17 after FDR correction, q<0.05). This translates to 9-49% mortality risk reduction per additional var. *rudis* drought allele. This architecture—combining detectable moderate-to-large effect loci with genome-wide background effects—demonstrates the complex genetic basis of drought adaptation in *A. tuberculatus*.

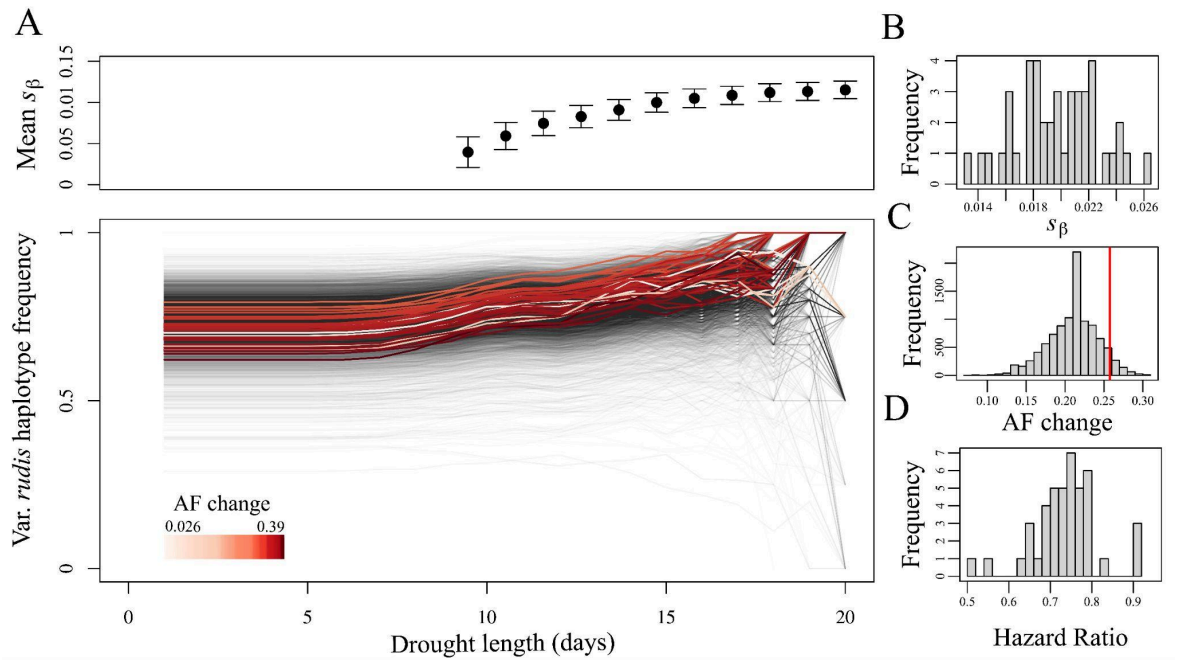

Fig. 4. The genomic impact and tempo of drought adaptation across an extreme drought event. (A) (lower panel) The frequency of var. *rudis* haplotypes over the course of the drought experiment, with the frequencies at day 0 representative of the distribution of ancestry among all contemporary samples. Red lines denote the 43 focal loci (after performing the LD-based clumping algorithm), colored by allele frequency change ($AF_{t=20}$-$AF_{t=0}$). Black lines reflect 10,000 randomly selected sites to illustrate genome-wide trajectories. (upper panel) The mean survival-based selection coefficient (s_β) for the 43 drought loci initially increases with drought duration but shows a threshold effect. **(B)** The mean allele frequency change ($AF_{t=20}$-$AF_{t=0}$) for the 43 drought-adapted alleles (mean for data = 0.26, red bar) is significantly elevated compared to the genome-wide null expectation (gray distribution; p-value = 0.05). The null was obtained by randomly selecting 43 alleles with the same starting allele frequency distribution, and calculating the mean frequency change for each set, 10,000 times. **(C)** Within-generation survival-based selection coefficients (s_β) for each drought-associated locus over the course of the entire drought experiment (mean = 0.12, std = 0.012). **(D)** The distribution of Cox hazard ratio values across drought-related loci indicate substantial protective effects of s drought-associated that vary by nearly 2 fold.

Century-long dynamics of modern drought-loci in response to climate

To study the dynamics of polygenic drought adaptation over the last century, we leveraged herbarium specimens spanning 120 years of changing climate. This collection of 87 previously sequenced herbarium specimens (19) were sampled between 1880 to 2011, and span most of the geographic native range of waterhemp (**Fig. 1A**). After fine-scale ancestry inference in these historical samples, we found 680 drought-tagging loci in common with the GWAS, resulting in 33 independent loci after LD-clumping. We analyzed change in these loci alongside NOAA records of maximum temperature and total precipitation in waterhemp's summer growing season dating back to 1880 (see *methods*, **Fig. S11**).

To investigate whether loci underlying drought-tolerance show evidence of adaptive tracking across timescales, we tested whether changes in allele frequency correlated with climate change through time. To reduce the impact of spatial variation, we analyzed pairs of individuals that were geographically close (<100km, **Fig. 5A**) but spanned distinct temporal intervals (ranging from 1 to 111 years apart, **Fig. 5B**), calculating Spearman correlations (ρ) between change in max growing season temperature or change in total summer precipitation and allele frequency change across the 31 drought loci with sufficient data. A Wilcoxon signed-rank test revealed that the distribution of ρ was significantly shifted toward positive values for temperature (p-value = 0.003, **Fig. 5C**), but not precipitation, indicating systematic increases in drought-protective alleles under warming conditions and decreases under cooling conditions. Permutation tests (randomizing temperature amongst genotypes) showed that a result at least this extreme occurred 5% of the time under null expectations (permuted p-value = 0.05). However, other correlation metrics showed somewhat more marginal significance, with 3/31 loci showing significant positive correlations compared to the ~0.8 expected by chance (permuted p-value = 0.07) and a median correlation coefficient of 0.16 across all loci (permuted p-value = 0.09). Together, these findings suggest drought alleles show modest evidence for adaptive tracking of temperature, increasing and decreasing as temperature varies through time but with heterogeneous responses across loci.

To gain a comprehensive understanding of the spatiotemporal dynamics of drought adaptation over the last century, we modelled how the collective change in frequency of drought alleles through time and space depends on climate. To do so, we implemented logistic and linear multivariate models of drought allele frequencies that included year, year by maximum growing season temperature, year by total precipitation in the growing season, latitude, longitude, and locus-specific effects. The linear analysis revealed significant effects of several predictors (**Table S4**) including the interaction between growing season max temperature and year ($F_{1,1088}$ = 8.70, p-value = 0.003), indicating that the linear rate of annual allele frequency change is modulated by the temperature experienced in each specific year (**Fig. S12**). Based on the logistic model, this temperature effect corresponds to a selection coefficient (*s*) of 0.028 [SE = 0.016] for the highest growing season max. temperature regime (45°C) and *s* = -0.040 [SE = 0.016] for the lowest growing season max. temperature regime (25°C) over the last century (temperature x year effect; X^2 = 4.71, p-value = 0.03).

However, this temperature-driven pattern changed when we considered collection context. After accounting for whether herbarium accessions were found in natural or agricultural settings—which covaries with both temperature and precipitation conditions (**Fig. S13)**—precipitation rather than temperature became the strongest predictor of the linear rate of allele frequency change through time ($F_{1,1002}$ = 4.35, p-value = 0.037, **Fig. 5D)**. Furthermore, the temporal response was marginally habitat dependent ($F_{2,1002}$ = 2.98, p-value = 0.05), with agricultural populations showing faster allele frequency change through time along with higher baseline frequencies than populations in natural habitats ($F_{2,1002}$ = 2.97, p-value = 0.052). After controlling for these predictors, we found that the frequency of drought alleles also significantly differed by locus ($F_{32,1002}$ = 1.47, p-value = 0.049), precipitation ($F_{1,1002}$ = 4.49, p-value = 0.034), longitude ($F_{1,1002}$ = 8.12, p-value = 0.0045) and latitude ($F_{1,1002}$ = 30.12, p-value = 5.13×10^{-8}), with every degree of latitude increasing the frequency of drought alleles by 6.42%, highlighting the consistent spatial structuring of adaptive variation in response to climate gradients across the landscape. A logistic model recovered weaker signatures of climate-dependent allele frequency change once accounting for collection habitat (growing season cumulative precipitation x year: X^2 = 2.34, p-value = 0.13) but were consistent in directionality, with s = +0.015 [SE = 0.010] and s = -0.027 [SE = 0.018] for 50 mm and 850 mm cumulative growing season precipitation regimes, respectively, and with spatial predictors remaining as significant predictors (latitude X^2 = 15.28, p-value = 0.0001, longitude X^2 = 4.16, p-value = 0.041). Overall, these models provide evidence for fluctuating selection on drought tolerance loci, increasing in frequency under hot/dry conditions, and decreasing under cool/wet conditions, with human-mediated selection in agricultural environments modulating these climate-driven evolutionary responses.

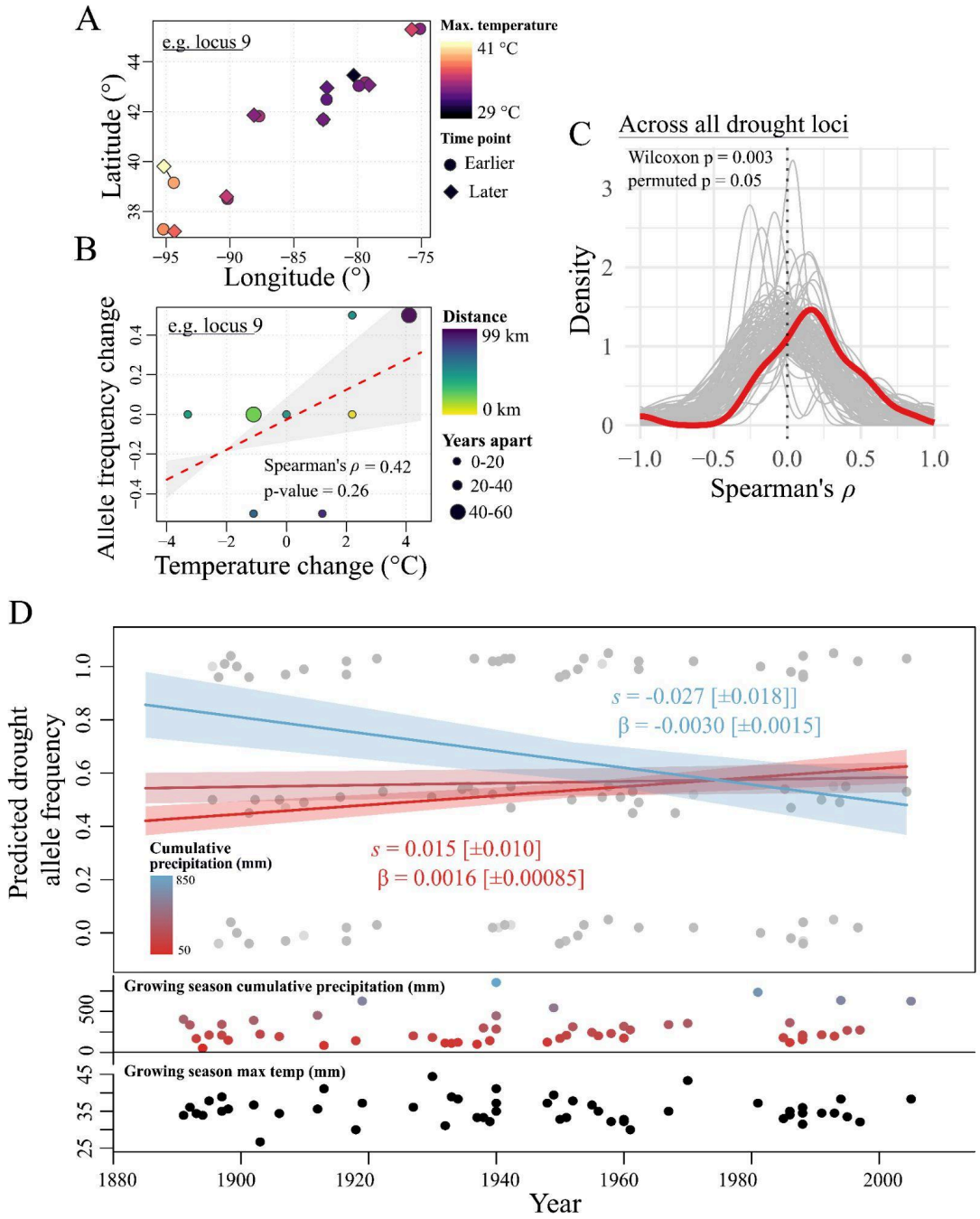

Fig. 5. Climate-tracking of drought-adapted alleles across timescales. (A-C) Evidence of climate tracking based on correlated shifts in the frequency of drought alleles and maximum temperature (°C) in the growing season between spatially-paired herbarium samples. (A) Samples are paired by minimizing distance (km) and proportion of missing data per locus, as exemplified here with drought locus 9. (B) The Spearman's correlation coefficient between temperature change (°C) and allele frequency change is calculated for each set of pairs at each locus, again, exemplified here with drought locus 9. (C) The resulting distribution of Spearman's correlation coefficient observed for 33 herbarium-matched drought loci (red) as compared to a null distribution from permutations randomizing climate with respect to sample (maintaining genotype and temporal structure). (D) The collective trajectory of drought loci (predicted allele frequency through time) is precipitation dependent—with evidence of positive selection in dry years and negative selection in wet years. Predicted values inferred from both linear (β) and logistic (*s*) multivariate regressions, controlling for geographic and environmental variables along with year and climate. Growing season cumulative precipitation (mm) and growing season maximum temperature (°C) corresponding to each spatiotemporal sample is illustrated below.

Discussion

As global warming intensifies both the severity and frequency of drought events (55), understanding how these changes affect genome-wide diversity within and across populations becomes increasingly critical for conserving and managing biodiversity. To address this challenge, we investigated the genetic architecture and evolutionary dynamics of drought adaptation across the landscape using the native plant turned agricultural weed, *Amaranthus tuberculatus.* We discovered that variation in drought tolerance correlates with habitat type, geographic location, and ancestry whereby plants from southwestern populations, agricultural habitats, and of var. *rudis* ancestry survive longer under water stress. By leveraging this ancestry-structured phenotypic variation, we identify a polygenic basis for drought adaptation, with drought-related loci distributed across nearly all chromosomes and exhibiting signatures of strong directional selection under extreme seasonal drought events. While this pattern suggests that substantial genome-wide diversity should be depleted under intensifying drought regimes, herbarium genomic analysis of these drought-adapted loci over the past 130 years reveals a signature of fluctuating selection. Collectively, drought-responsive loci exhibit a climate-dependent pattern of selection over time—selected for during hot/dry years but against during wet/cool years—with individual loci varying in their degree of climate-tracking. This dynamic deployment of standing variation suggests that landscape-level variation in anthropogenic selection pressures—including both agricultural practices and drought intensification—can maintain adaptive diversity across spatiotemporal scales.

When environments change rapidly, polygenic responses are expected to draw substantially on standing genetic variation, which facilitates adaptation by enabling more substantial phenotypic shifts than relying on new mutations alone (56–59) (60). While population structure can confound the detection of polygenic architectures (32, 61), here we leverage a strong ancestry-specific response—explaining 33% of the variation in drought tolerance—to map this standing variation and understand the processes that maintain it. Our inference of ancestral haplotypes revealed that ongoing admixture and recombination have broken down large ancestry blocks into fine-scale segments, enabling precise mapping. Admixture mapping identified a polygenic basis for drought adaptation, involving 43 loci across 13 chromosomes (**Fig. 3**), with polygenic scores further revealing substantial variation in the architecture of drought adaptation among individuals. We expect that this variation has been shaped by both the demographic processes that influence the spread of standing variation across landscapes (such as the recent northwestern expansion of var. *rudis*) (19, 39) and the adaptive evolutionary processes that maintain them through space and time.

To understand how rapidly variation at these alleles could be lost to selection, we measured the strength of selection acting on these loci during an experimentally-imposed seasonal drought event. During a lethal drought lasting ~3 weeks, we detect strong directional selection across 43 loci; these regions increase more rapidly than other frequency matched ancestral haplotypes across the genome, at a rate (s_β) of about 12% per day on average (**Fig. 4**). This estimate is akin to a standard selection coefficient for the homozygous alternate

genotype, but differs in that it reflects the within-generation as opposed to across-generation fitness advantage. These rapid evolutionary responses may be enabled by the remarkably large census and estimated contemporary effective population sizes in waterhemp – a common feature of successful agricultural weed species (62, 63). Previous work estimated that European *A. thaliana* populations would need selection coefficients (*s*) of 1-3% to track predicted 2070 climate conditions (32). While our observed rates suggest that the hyper-diverse waterhemp can mount the evolutionary responses needed for climate tracking, the critical question is whether such selection strength can be sustained across complex landscapes over decadal timescales.

To quantify these evolutionary dynamics, we examined drought adaptation across spatiotemporal scales using herbarium and climate records. At a century-long scale, drought allele frequency dynamics reflect fluctuating selection from a changing climate, with an $s \sim +0.028/+0.015$ in warmest/driest regimes and -0.04/-0.027 in coolest/wettest regimes. This pattern of fluctuating selection is consistent with fitness costs resulting from drought adaptation, as seen in other systems and agricultural weeds (36, 64, 65). Experimentally, we find mixed evidence of growth-related tradeoff, where populations (but not individuals) with higher drought-LD_{50} grow more slowly, although this scale-dependent relationship could also reflect correlated selection between drought and extended season length to grow more slowly by for longer in southwestern, var. *rudis* localities. This complexity highlights the challenge of detecting fitness costs that may be subtle, environment-specific, or operate through pathways beyond simple growth-survival tradeoffs (66–68). When examined through spatially matched temporal comparisons ranging from 1-111 years (mean difference = 48 years, SE = 4.77 years), herbarium specimens demonstrated somewhat attenuated evidence for adaptive tracking of drought loci with respect to temperature (**Fig. 5**). This adaptive lag at intermediate scales likely reflects additional factors that can buffer evolutionary responses, such as the substantial seed banks and extended dormancy that allow waterhemp seeds to remain viable up to 15 years (41, 69). Overall, fluctuating climate along with pleiotropic costs appears to be key to the maintenance of variation on which selection in contemporary landscapes acts, allowing populations to respond rapidly to environmental shifts (1, 70).

The scale of the genomic response to drought adaptation likely reflects the complexity of underlying ecological and physiological mechanisms involved. Drought adaptation typically involves escape (early life cycle completion), avoidance (water loss optimization), and tolerance (ability to handle low water potential) (27, 71). These strategies can be under the control of few large effect loci, like in drought-escaping *Panicum hallii (72)*, while a suite of complex traits and accompanying polygenic variation may underlie them in systems such as *Arabidopsis* and *Fragaria* (32, 73, 74). In our experiment, several loci with the strongest associations to drought tolerance – the homozygous genotype experiencing a fitness advantage of 0.14 per day on average – was linked to *DDB1*, a protein involved in the abscisic acid hormone signalling pathway and an important actor in the response to abiotic stress and drought escape in *A. thaliana (51, 75)*. Population-level analyses do not support a positive correlation between growth and drought adaptation (**Fig. 1E**, **Fig. S4**), suggesting escape may not be a foremost driver of drought adaptation in waterhemp. With 42 additional

loci showing detectable associations (some broadly involved in the abiotic stress response: *RKD* (49)*, PER17* (48), *TCD2 (50)*) and genome-wide ancestry retaining predictive power after controlling for these loci, our results suggest a mixed-effect architecture underlies drought tolerance in waterhemp (as in (76)), with both large effect loci and here unresolvable small-effect allelic contributions. Future work may look to resolve the extent to which individual genetic variants contribute to escape, avoidance, or resistance mechanisms, and the role of pleiotropy in this genetic architecture (73, 77).

For many native plants like waterhemp, adaptation to fluctuating climate must occur alongside the conversion of their habitat to agriculture. In cropping systems, high plant densities and soil compaction can reduce water availability, thereby intensifying selection from drought in largely unirrigated landscapes such as the Midwestern Corn Belt (78, 79). Our selection experiment demonstrates that agricultural populations tend to be better adapted to water limitation than natural populations, surviving longer under drought. Genomic time series analysis further resolves both a difference in drought allele frequency among habitats and stronger selection on drought alleles through time in agricultural compared to natural habitats. However, both these phenotypic and genomic dynamics could result from either increased drought pressure in agricultural systems or reduced drought selection in natural populations, which are often riparian habitats with high water availability. Given var. *rudis*' historical association with, disturbed habitats, Sauer suggested it may be better adapted, or even "preadapted", to agricultural habitats (39), a hypothesis supported by recent phenotypic and genomic work (19, 40). Notably, all 43 loci identified to have protective effects under drought in this study were derived from var. *rudis* ancestry (**Fig. 4A**), and are enriched in agricultural populations beyond genome-wide expectations (**Fig. S10**), consistent with experimental phenotypic data showing longer survival of *rudis* types and agricultural populations under drought (**Fig. 2**). Although we have yet to test the role of disturbance in preadaptation to agriculture, the results here, along with divergent climate histories across ancestries (80) suggest that adaptation to drought has been particularly important in var. *rudis*' and waterhemp's invasion into agriculture.

Waterhemp's dynamics of drought adaptation reinforces a fundamental tension: while populations can rapidly evolve under extreme selection, heterogeneity across space and time buffers these responses over larger spatiotemporal scales. Our experiments demonstrate the substantial standing genetic variation that facilitates rapid adaptive responses to drought, in part due to fluctuating selection preventing its erosion. As climate change accelerates and drought intensifies, whether directional selection will overwhelm this heterogeneity needed for climate tracking remains an open question. Understanding these multi-scale dynamics across species will be critical for predicting evolutionary outcomes under accelerating environmental change.

Acknowledgements

Thank you to Tyler V. Kent, Sally P. Otto, Maryn Carlson, along with the Reiseberg, Carley, and Kreiner labs for feedback and input on various stages of this work. We appreciate the efforts of the UBC Hortical Greenhouse staff and undergraduate research assistants, Camila Cordova and Vicky Lim, for help with implementing the drought experiment.

Data Availability

Sequencing data and code corresponding to analyses presented here will be made publicly available on Genbank and Github at the time of publication.

Methods

Drought selection experiment

This experiment drew from collections of 34 *Amaranthus tuberculatus* populations, sampled in design pairing nearby natural and agricultural habitats across the Midwestern United States (17 pairs total; Kreiner et al. 2021). We used seeds from 490 maternal lines from a subset of 24 populations (12 agricultural, 12 natural; **Fig. 1A**). For each maternal line, two replicates of 10 seeds were sown into separate soil discs in a growth chamber under a fluctuating temperature regime (28°C day / 18°C night) for 10 days, providing one replicate for each of two treatment groups.

Seedlings were then transplanted into 1L pots filled with Sunshine Mix #4 (Sun Gro Horticulture) and moved to the University of British Columbia agriculture greenhouse. With 490 lines x 2 treatments, the experiment included 980 pots/individuals in total. Pots were distributed in a randomized block design across two greenhouse benches. The experiment was conducted from July through August. Day length matched the natural photoperiod during this time, but full-spectrum lights were activated in the greenhouse during cloudy periods throughout the day. Late-emerging seedlings were thinned to ensure a single focal plant per pot.

Water was delivered to control and treatment pots via automated dripper lines, supplying 100 mL every 6 hours (400 mL/day) for the first three weeks of growth. During this period, two leaves per plant were collected for later DNA extraction. At three weeks, irrigation lines to all drought treatment pots were shut off completely. Stem width and plant height were measured for all plants immediately before drought onset and again 2 weeks post-treatment. Plant survival was monitored daily, and individuals were considered dead at the point of full wilting—defined as complete loss of turgor pressure in apical and leaf tissues. When this occurred, the date of death was recorded and the individual was removed from the experiment. This design enabled us to quantify both drought tolerance and growth potential, facilitating tests for trade-offs between these traits across natural and agricultural populations.

Phenotypic Analysis of Drought

We measured drought tolerance using the day to full wilt (phenotype described above). We employed two complementary statistical approaches to analyze variation in drought tolerance. First, we used an individual-level mixed effects regression models to examine survival while controlling for experimental features. Second, we analyzed survival curves using a generalized linear model applied to grouped data. For the survival curve analysis, we binned individuals into four longitudinal groups (using cut breaks at -96, -93, -90, -86, and -82 degrees longitude) and two environment types (agricultural vs. natural), then calculated the proportion of individuals surviving each day following the onset of drought. The quasibinomial family was selected to account for overdispersion in the proportional survival data. We added zero values for days when no mortality was observed within specific longitude-environment combinations to create complete survival curves. Both models

included main effects and interactions between longitude and environment, with the individual-level model additionally incorporating random effects for block structure (bench nested within tray) and covariates for initial stem width and height growth rate. All analyses were conducted in R using the *car* package for Type II/III ANOVA tests and *lsmeans* for post-hoc comparisons.

To further assess variation in population-level drought resistance, we calculated the proportion of surviving samples for each population for each day of the drought experiment. These population survival curves were constrained to start at 100% survival on day 1 and 0% on day 20 when all individuals had died (**Fig. 1B**). To model the dynamics of survival through time, we fitted survival curves with a logistic function using the *nls* and *SSlogis* functions in R (see **Fig. S2** for example and equation). From the estimated parameters, we calculated the lethal dose, defined as the day when 50% of the population has died (LD_{50}). To quantify predictors of phenotypic variation in drought tolerance, we implemented a multiple regression model of LD_{50} against habitat, longitude and latitude. The partial R^2 for each variable of interest was estimated removing it from the model and subtracting the reduced model multiple R^2 from the full model multiple R^2. Additionally, we applied a non-parametric test of whether LD_{50} differed between habitats using a permutation approach. We permuted 10,000 times the habitat assignment for each population, and calculated the difference between the mean LD_{50} in agricultural versus natural habitats (**Fig. S3)**. In addition, to test for the effect of habitat on drought resistance, we performed a one-sided Wilcoxon rank test with paired samples with *wilcox.test* function in R (**Fig. 1D**).

DNA collection and sequencing

Genomic DNA was extracted from 300 samples using a modified CTAB protocol (81, 82). Briefly, frozen tissue was ground and subjected to a two-step extraction with CTAB-free buffer followed by 3% CTAB buffer supplemented with β-mercaptoethanol. After chloroform extraction, DNA was precipitated with isopropanol, washed with ethanol, and treated with RNaseA. The purified DNA was quantified using a Qubit fluorometer, with 280 samples yielding sufficient high-quality DNA (≥1 ng) for library preparation following the drought treatment. Illumina paired-end libraries were constructed using a protocol largely modified from (83), the TruSeq DNA Sample Preparation Guide from Illumina (Illumina, San Diego, CA) (84). Genomic DNA (1 ng) was sheared to approximately 350 bp using a Covaris ultrasonicator with the following settings: Peak Incident Power 50, Duty Factor 20%, Cycles per Burst 200, Treatment time 65 s, at 20°C. Size selection was performed using a two-step SPRI bead purification protocol with home-made SPRI beads (84), optimized to select for 350 bp fragments.

The size-selected fragments underwent end repair using NEBNext End Repair enzyme mix, A-tailing with Klenow Fragment (3'→5' exo-), and adapter ligation with NEB Quick Ligase using P1 and P2 adapters (with unique barcodes for each sample). Libraries were enriched by PCR amplification using KAPA HiFi HotStart ReadyMix with 8 PCR cycles. The amplified

libraries were purified using SPRI beads and eluted in Tris buffer (pH 8.0, 10 mM). Library quality was assessed using a Qubit fluorometer (High Sensitivity kit) and fragment size distribution was verified on a Bioanalyzer (High Sensitivity DNA chip), with successful libraries showing concentrations ≥5 ng/µl and peak sizes of approximately 470 bp (including ~120 bp adapter sequences). Sequencing was performed at Novogene on 4 lanes of a NovaSeqX 25B.

Genome alignment and variant calling

Raw sequencing reads were processed using fastp v0.23.2 for adapter removal and poly-Q tail trimming. Quality-filtered reads were aligned to *Amaranthus tuberculatus* reference genome (haplotype 2 of accession 19_3; (85)) using BWA-MEM v0.7.17 with default parameters and appropriate read group headers, and alignments were converted to BAM format and sorted using samtools v1.15.1 with multi-threading enabled. PCR and optical duplicates were identified and marked using Picard MarkDuplicates v2.27.4. Read processing procedures were as above for historical herbarium samples, but with three modifications to account for DNA degradation. DNA damage patterns were assessed and corrected using mapDamage (86) with the --rescale option to account for typical cytosine deamination patterns in historical samples, paired-end reads were merged with fastp due to small fragment size distributions, and duplicates were called with a program DeDup which is optimized for aDNA (87).

We called genomic variants using FreeBayes v1.3.6 in parallel across 100kb genomic regions, separately for the contemporary and herbarium sample datasets. FreeBayes was run with the --use-best-n-alleles 2 and --report-monomorphic flags to call both variant and invariant sites. Variant calling was parallelized across multiple compute nodes using GNU Parallel. Raw variants were processed separately for SNPs and invariant sites using bcftools. For both site types, we applied an initial filter requiring ≤25% missing data across samples (F_MISSING <= 0.25). SNPs underwent additional quality filtering including: minimum variant quality score ≥30 (QUAL >= 30), allele balance between 0.25-0.75 for heterozygotes or ≤0.01 for homozygotes (AB >= 0.25 & AB <= 0.75 | AB <= 0.01), presence of reads on both forward and reverse strands (SAF > 0 & SAR > 0), minimum mapping quality ≥30 for both variant and reference alleles(MQM >=30 & MQMR >= 30), and paired-read support criteria. Only biallelic SNPs with allele frequencies between 0 and 1 were retained for downstream analyses.

Investigations of Trade-offs with Drought Tolerance

To test whether drought tolerance showed evidence of trade-offs with growth rate or herbicide resistance, we compared traits at the individual-level and population-level, in univariate and multivariate models (**Fig. S5**).

For drought tolerance trade-offs, the day of full wilt was used for individual-level analyses, and drought LD_{50} for population-level analyses. We quantified growth rate by measuring plant height before the drought treatment, along with one week and two weeks after in both control and drought-treated plants. We estimated resistance to glyphosate herbicides by quantifying depth at the EPSPS locus, as in (88). For each sample, we thus calculated depth within the EPSPS gene using mosdepth (89), which we then normalized by dividing by the mean genome-wide depth at coding sites.

Trade-offs were modeled at the individual and population-levels initially with univariate models (where for drought tolerance, this was represented by day to full wilt and drought LD_{50}, respectively). We tested whether growth rate in drought-treated plants predicted that individual's drought tolerance, along with how the growth rate in its sibling in the control treatment predicted its drought tolerance (showing only the latter in **Fig. 1E**). We further implemented multivariate models for growth, herbicide and drought resistance as independent variables. At the individual-level, we tested the effects of experimental settings (bench and tray, height when drought treatment was imposed), geography, habitat and ancestry (growth/herbicide or drought resistance ~ Bench/Tray + longitude + latitude + habitat*mean ancestry). At the population-level, we accounted for geography, habitat and mean ancestry effects (growth/herbicide or drought resistance ~ Bench/Tray + longitude + latitude + habitat*mean ancestry). Finally, we implemented a model to test the effects of growth, herbicide resistance, geography and habitat on drought resistance at the individual and population levels (day of full wilt/LD_{50} ~ growth rate + herbicide resistance + habitat + longitude + latitude).

Genome-wide population structure and its relationship to drought tolerance

We used PLINK (version 2024.04.1+748) (90) to perform a PCA of genotypes on a thinned set of SNP to reduce effects of linkage disequilibrium (**Fig. 2A**). To control for LD among samples, we performed LD thinning by calculating LD between each SNPin 100-kb windows across the genome, using a step size of 10kb, removing SNPs with an LD (r^2) >0.5. We detected two outlier individuals on our initial PCA, that formed a very distinct group from the rest of the samples. We speculated that they might be another species of *Amaranthus* and dropped these two samples from the rest of the analyses. We then used ADMIXTURE (version 1.3.0) (44) to calculate global ancestry with k=2 (**Fig. 2A**). For plotting, samples were ordered by longitude. We then calculated the proportion of var. *rudis* ancestry by individual and population based on the genomic proportion derived from the ancestral grouping with higher frequency in the southwest, for later use in regression analyses against drought tolerance.

To test the effects of genome-wide ancestry (in addition to geographic, and environmental predictors) on the population-level drought LD_{50} estimates, we extended our multiple linear regression models to include ancestry as a covariate: drought LD_{50} ~ longitude + latitude + habitat + longitude*k-based ancestry estimate (**Fig. 2C**). Additionally, we tested the effect of ancestry using PC1 as a proxy for ancestry: drought LD_{50} ~ longitude + latitude + habitat +

longitude*PC1. The interaction between longitude and habitat was dropped because it was not significant. As above, partial R^2 for variables of interest was calculated by subtracting the multiple R^2 value of a reduced model without ancestry as a covariate from the multiple R^2 value for the full model. Further, when we expand our quasibinomial model of days to survival based on data grouped into four longitudinal bins and two environments to include ancestry (**Fig. 1B**), we also resolve a significant ancestry effect ($X^2 = 3.86$, p-value = 0.049), with the habitat, longitude, habitat:longitude, and early growth rate remaining as significant predictors.

Local ancestry inference

To infer ancestry at each position in the genome, we used AncestryHMM (91). This approach requires (1) the allele counts for each of the parental ancestry panels (*var. rudis and var. tuberculatus*), (2) the recombination distance between each locus, and (3) the genotype call for each focal sample at each ancestry informative site.

To generate allele accounts for the ancestry panels (1), we used an independent and previously generated dataset (40) selecting pure var. *rudis* and var. *tuberculatus* populations for the two ancestry panels. To determine which individuals were of pure ancestry, we mapped reads to the newest reference genome version (85) and called and filtered SNPs as above before running ADMIXTURE (version 1.3.0) assuming k=2. We identified 44 pure *var. rudis* and 21 pure *var. tuberculatus* samples using a threshold of 0.00001 alternate ancestry. We filtered the variant file (50,811,811 SNPs) for this set of samples and applied a minimum allele frequency cutoff of 0.05. To identify ancestry-informative sites, we calculated F_{ST} using VCFtools (version 0.1.16) on a site-by-site basis, and retained variants as ancestry informative if their F_{ST} fell above the 75th percentile (2,089,620 variants). We intersected these sites with SNPs from the drought selection experiment, resulting in 788,177 sites. Finally, we extracted population-level allele counts for each ancestry grouping for each site using a custom bash script.

To generate the linkage map for (2), we used a set of scripts https://github.com/QuentinRougemont/LDhat_workflow using the interval algorithm. We used a precomputed look-up table based on theta=0.01, n=100. We then estimated *r* between SNPs from the ldhat output based on rho = $4N_e r$ with N_e = 540,804 as estimated in (88). Then, we fit a monotonic spline on the cumulative distribution of these recombination rates, to calculate the physical distance along the chromosome and between each ancestry informative SNP in the drought variant call set presented in (1). Finally for step (3), we extracted the read count for each ancestry informatic site for each focal sample in the drought dataset from the filtered variant file using a custom bash script (788,177 variants and 280 individuals).

We ran ancestry_hmm model with overall ancestry proportions of 33% of var. *tuberculatus* and 67% *var. rudis*, based on the mean of ADMIXTURE estimates across our accessions. We modelled two pulse events that introgressed *var. rudis* into *var. tuberculatus* with a prior of

10,000 and 100 generations ago. The resulting model predicted an initial pulse of var. *rudis* into var. *tuberculatus* of 42.54% 10,000 generations ago, followed by a more recent pulse of 24.56% 7.45 generations ago. We assigned ancestry based on probability outputs from the model with a cutoff of 0.9 (NA below that threshold). Probabilities were given for how many *var. rudis* allele was derived from pulse one or two. Since we were only interested in the ancestry genotype (rather than pulse-specific origin), we summed across pulses to obtain the count of *var. rudis* alleles (0, 1, or 2) for each individual at each locus.

Admixture mapping

To detect significant associations between loci across the genome and tolerance to drought, we conducted a Genome Wide Association Study (GWAS) with the day to full wilt/survival under drought as the dependent variable. We evaluated models based on qqplots (software package) to identify a suitable approach for our analysis. Since drought tolerance is highly correlated with ancestry, the risk of false positives with a SNP based GWAS while controlling for structure was high. To address this, we conducted GWAS on ancestry calls after filtering out loci with > 20% missing data, with an ancestry-based relatedness matrix as a covariate. We applied a genomic inflation factor ($\lambda = 2.35$) to correct for an overrepresentation of significant variants with low -log10(p-values). FDR correction was applied to p-values, with a threshold of $q = 0.05$ indicated on **Fig. 3B**.

To identify independent drought-associated variants, we performed LD-clumping on SNPs that passed the q=0.05 threshold. To do so, we used plink --clump, dropping SNPs with an $r^2 > 0.5$ with a focal index SNP within a 100 kb window. For these focal drought variants, we then extracted their GWA effect size (β), genotype frequency, and p-value. We calculated the individual polygenic scores based on the sum of the products of genotype frequency (0,0.5,1) and β at each loci (92). These scores were then used to estimate the joint effect of drought-adapted loci on survival probability (see *methods* on *hazard ratio*).We used bedtools intersect to identify genes that drought-associated SNPs mapped to. Using both the de novo annotation file and *Arabidopsis* orthologues identified with orthofinder2 (93), we identified a set of genes for GO enrichment analysis using PANTHER 19.0 (**Table S3**) (94). To link genes to function, we searched the literature for evidence of drought implication of the most important SNP hits in our dataset (**Table S2**). We also used snpEff (95), with a custom *Amaranthus* database, to identify the type and effect of mutation on the protein sequence.

Within-generation survival-based selection coefficients (s_β), allele frequency change, and Cox hazard analyses

To determine the strength of selection in our drought experiment, we fit a logistic model to the daily change in individual haplotype frequency during the drought survival experiment. To do so, we first calculated daily haplotype frequencies using genotype assignments from the ancestry mapping analysis, combined with the survival data from the drought experiment. Genotype value was rescaled to allele frequency, encoded as 0 (var. *tuberculatus* homozygote), 0.5 (heterozygote) or 1 (var. *rudis* homozygote) (**Fig. 4A**). Missing genotypes

(./.) were excluded from frequency calculations. To fit a logistic model to these allele frequency trajectories through time, we further scaled individual genotypes by whether or not an individual was observed on each day. Critically, individuals were coded as missing (NA) for all days following their day they died to avoid artificially deflating selection coefficients by including dead individuals in frequency calculations. For each locus separately, we regressed this vector of individual genotypes remaining in the experiment on when they were observed using the *glm* function in R with the *"family=binomial"* option (formula: scaled genotype ~ day). The slope of this model represents the change in logit-transformed allele frequency per day of drought treatment, reflecting differential survival favoring drought-adapted alleles. When additivity is assumed, 2 x slope = s_β, reflecting the fitness advantage of the homozygous alternate genotype. Unlike traditional selection coefficients estimated from frequency changes across generations, this within-generation coefficient (s_β) directly measures selection as it occurs during the drought event, isolating the selective pressure from confounding demographic processes (**Fig. 4B**).

To test whether the increase in drought-adapted loci frequency over the course of the experiment was enriched relative to the genome-wide background, we implemented the following permutation procedure. We first selected a set of 43 loci that had the same starting allele frequency distribution (binned precision of 0.003) from the full set of ancestry-informative loci (>700,000 sites) as our set of 43-drought adapted loci. We calculated the mean change in allele frequency between the first and last day of the selection experiment for each set. We repeated this procedure 10,000 times to generate the null expectation of mean allele frequency change in our drought experiment (**Fig. 4C**). Statistical significance was assessed by calculating the proportion of permuted means that exceeded the observed mean frequency change.

To evaluate the protective effects that each drought-associated locus confers in reponse to drought, both individually and collectively, we implemented Cox proportional hazards regression models using the function *coxph* in R. We first fit a separate model for each locus with ancestry as a covariate, applying a FDR correction to the p-values to correct for multiple testing (**Fig. 4D)**. We then fit a model to the PGS with ancestry as a covariate. Protective effects against drought per unit predictor (k) was calculated as $1\text{-}HR^k$.

Relating Adaptation to Agriculture to Drought Tolerance

To identify loci divergent between habitats, we implemented a Cochran-Mantel-Haenszel (CMH) test with plink on genetic variants from the drought sequenced samples, enabling the detection of loci consistently enriched in a given habitat across our replicate paired habitat design (as in (19)). To identify which loci from the set of 893 drought-adapted loci (before clumping) were significantly divergent between habitats, we took the intersection of significant loci from the drought-tolerance GWAS and CHM scan. Due to the large number of loci passing the FDR threshold in the CMH scan, we selected a threshold (α=0.015) that maximized both the number and proportion of shared loci between GWAS and CMH results (**Fig. S7**). Using this approach, we identified 13,602 loci from the CMH scan, with 43 (out of

893) being significantly associated with drought and divergent between habitats. To estimate the enrichment of drought alleles depending on the environment (**Fig. S8**), we sorted the samples by habitat (143 and 137 samples for agricultural and natural, respectively), and calculated the mean ancestry per locus for the 43 drought adapted loci.

To test whether drought alleles were particularly enriched in agricultural compared to natural habitats, we first estimated individual level drought-allele frequency by averaging genotypes across the 43 previously identified drought-associated loci. We fitted a linear model predicting drought-adapted ancestry as a function of environment, latitude, longitude, and their interactions, while controlling for genome-wide ancestry proportions (as inferred from ADMIXTURE) as a covariate. Model significance was assessed using Type III ANOVA. To visualize significant interaction effects, we generated least-squares means predictions across the range of observed latitudes (38.5–41.5°N) and longitudes (83–95°W), calculating the difference in predicted drought allele frequency between agricultural and natural populations at these geographic extremes.

Spatiotemporal Genomic Analyses of Climate Adaptation

To correlate climate to haplotype frequency change through time in the herbarium samples, we pulled data from the NOAA yearly climate database (https://www.ncei.noaa.gov/pub/data/ghcn/daily/by_year/, downloaded on 04/25/25) from across sample collection dates, from 1828 to 2011. We used a custom R script to identify the nearest NOAA weather station to each of our herbarium samples in the year of its collection. Since drought is associated with low precipitation and high temperatures and because *A. tuberculatus* is a summer annual, we extracted the maximum temperature (in Celcius) and total precipitation (in mm) across June, July, and August (representing climate conditions in its growing season). We removed samples where the closest weather station was more than 50 km from the samples locality resulting in 95 samples ranging from 1880 to 2011 (88 for precipitation and 59 for maximum temperature, **Fig. S11**). As in (19), habitat was assigned to herbarium samples based on annotations of habitat descriptions on the specimens.

Ancestry in herbarium samples was determined at each of 974,134 ancestry informative loci in the SNP set using ancestry_hmm with the same approach as described above. We then intersected ancestry calls in the herbarium dataset with the drought-associated loci (893 SNPs). We applied the clumping algorithm as above (100kb-windows, threshold on p-wald = 6.58×10^{-5}, $r^2 = 0.5$).

To analyze the dynamics of drought-adapted haplotype frequency change over a range of timeframes, we implemented an analysis that correlated change in climate to changes in genotype frequency among pairs of samples. This approach was designed to minimize the influence of spatial variation while maximizing the detection of temporal evolutionary responses to climate change. We first identified all possible sample pairs from our dataset, and ranked sample pairs by geographic distance, with the closest pairs prioritized for selection. For each drought-associated SNP, we used a greedy pairing algorithm that

prioritized geographically proximate samples while ensuring non-overlapping sample usage within each SNP analysis. The pair selection process involved several filtering criteria: pairs must span different collection years (year difference > 0), geographic distance must be ≤100 km between samples (calculated using Vincent ellipsoid distance), both samples in a pair must have non-missing genotype data for the focal SNP, and only SNPs with ≥3 valid pairs were included in analyses.

For each drought-associated SNP, we calculated the Spearman's rank correlation coefficient between temporal changes in drought allele frequency and climate between paired samples, separately for total growing season precipitation and growing season maximum temperature. Statistical significance was assessed through a permutation procedure that maintained the spatial-temporal structure of the genetic data while randomly reshuffling climate values among samples once per permutation. The same randomized climate dataset was used across all SNP analyses within each permutation. We calculated multiple test statistics including the number of significant positive correlations, the median correlation across SNPs, and the Wilcoxon signed-rank test. Permutated p-values were determined as the proportion of permuted datasets yielding test statistics equal to or more extreme than those observed in the observed data.

To quantify the collective trajectory of drought alleles through time depending on climate, we implemented linear and logistic multiple regression analysis. As climate has changed non-linearly through time, we were particularly interested in testing for interactions between year and climate variables (temperature and precipitation) while controlling for other covariates. We first tested a model of drought haplotype frequencies as a function of temperature, year and geographic coordinates (genotype frequency ~ temperature max*year + precipitation*year + loci + latitude + longitude). We then tested the effect of adding collection habitat to the model (natural/agricultural/disturbed) (genotype frequency ~ temperature max*year + precipitation*year + habitat*year + loci + latitude + longitude). Significance was assessed in all models with a type III ANOVA (*Anova* function in R). Predicted haplotype frequencies were calculated using the *lsmip* function, while the linear rates of change and logit transformed rates of change (selection coefficients) for these trajectories were extracted with the function *emtrend*.

References

1. P. W. Messer, S. P. Ellner, N. G. Hairston Jr, Can Population Genetics Adapt to Rapid Evolution? Trends Genet. 32, 408–418 (2016).

2. S. Yeaman, Evolution of polygenic traits under global vs local adaptation. Genetics 220 (2022).

3. J. T. Stroud, M. P. Moore, R. B. Langerhans, J. B. Losos, Fluctuating selection maintains distinct species phenotypes in an ecological community in the wild. Proc. Natl. Acad. Sci. U. S. A. 120, e2222071120 (2023).

4. R. D. H. Barrett, D. Schluter, Adaptation from standing genetic variation. Trends Ecol. Evol. 23, 38–44 (2008).

5. S. Yeaman, M. C. Whitlock, The genetic architecture of adaptation under migration-selection balance. Evolution 65, 1897–1911 (2011).

6. J. B. S. Haldane, A mathematical theory of natural and artificial selection. Math. Proc. Camb. Philos. Soc. 23, 363–372 (1926).

7. X. Wu, et al., Rapid adaptation and extinction across climates in synchronized outdoor evolution experiments of Arabidopsis thaliana. bioRxiv 2025.05.28.654549 (2025).

8. S. Busoms, et al., Fluctuating selection on migrant adaptive sodium transporter alleles in coastal Arabidopsis thaliana. Proc. Natl. Acad. Sci. U. S. A. 115, E12443–E12452 (2018).

9. A. O. Bergland, E. L. Behrman, K. R. O'Brien, P. S. Schmidt, D. A. Petrov, Genomic evidence of rapid and stable adaptive oscillations over seasonal time scales in Drosophila. PLoS Genet. 10, e1004775 (2014).

10. J. K. Kelly, The genomic scale of fluctuating selection in a natural plant population. Evolution Letters n/a (2022).

11. S. M. Rudman, et al., Direct observation of adaptive tracking on ecological time scales in Drosophila. Science 375, eabj7484 (2022).

12. M. C. Bitter, et al., Continuously fluctuating selection reveals fine granularity of adaptation. Nature 634, 389–396 (2024).

13. A. Troth, J. R. Puzey, R. S. Kim, J. H. Willis, J. K. Kelly, Selective trade-offs maintain alleles underpinning complex trait variation in plants. Science 361, 475–478 (2018).

14. J. M. Cocciardi, et al., The value of long-term ecological research for evolutionary insights. Nat. Ecol. Evol. 8, 1584–1592 (2024).

15. H. A. Burbano, R. M. Gutaker, Ancient DNA genomics and the renaissance of herbaria. Science 382, 59–63 (2023).

16. L. Eckert, I. Eckert, O. Rahn, C. P. So, R. D. H. Barrett, Using herbarium collections to study genetic responses to global change. New Phytol. (2025). https://doi.org/10.1111/nph.70454.

17. A. S. Kim, et al., Temporal collections to study invasion biology. Mol. Ecol. (2023). https://doi.org/10.1111/mec.17176.

18. J. M. Kreiner, et al., Rapid weed adaptation and range expansion in response to agriculture over the past two centuries. Science 378, 1079–1085 (2022).

19. P. L. M. Lang, et al., Century-long timelines of herbarium genomes predict plant stomatal response to climate change. Nat. Ecol. Evol. 8, 1641–1653 (2024).

20. P. Battlay, et al., Large haploblocks underlie rapid adaptation in the invasive weed Ambrosia artemisiifolia. Nat. Commun. 14, 1717 (2023).

21. O. L. Johnson, R. Tobler, J. M. Schmidt, C. D. Huber, Fluctuating selection and the determinants of genetic variation. Trends Genet. 39, 491–504 (2023).

22. G. Bell, S. Collins, Adaptation, extinction and global change: Adaption, extinction and global change. Evol. Appl. 1, 3–16 (2008).

23. N. J. Kooyers, et al., Population responses to a historic drought across the range of the common monkeyflower (Mimulus guttatus). Am. J. Bot. 108, 284–296 (2021).

24. L. M. McDonald, A. Scharnagl, A. K. Turcu, C. M. Patterson, N. J. Kooyers, Demographic consequences of an extreme heat wave are mitigated by spatial heterogeneity in an annual monkeyflower. Ecol. Evol. 13, e10397 (2023).

25. S. J. Franks, N. C. Kane, N. B. O'Hara, S. Tittes, J. S. Rest, Rapid genome-wide evolution in Brassica rapa populations following drought revealed by sequencing of ancestral and descendant gene pools. Mol. Ecol. 25, 3622–3631 (2016).

26. M. Exposito-Alonso, et al., Genomic basis and evolutionary potential for extreme drought adaptation in Arabidopsis thaliana. Nat. Ecol. Evol. 2, 352–358 (2018).

27. M. Exposito-Alonso, et al., Natural selection on the Arabidopsis thaliana genome in present and future climates. Nature (2019). https://doi.org/10.1038/s41586-019-1520-9.

28. M. Exposito-Alonso, Understanding local plant extinctions before it is too late: bridging evolutionary genomics with global ecology. New Phytol. 237, 2005–2011 (2023).

29. A. K. Mishra, V. P. Singh, A review of drought concepts. J. Hydrol. (Amst.) 391, 202–216 (2010).

30. A. M. Siepielski, et al., Precipitation drives global variation in natural selection. Science 355, 959–962 (2017).

31. R. E. Kramp, et al., Functional traits and their plasticity shift from tolerant to avoidant under extreme drought. Ecology 103, e3826 (2022).

32. N. J. Kooyers, The evolution of drought escape and avoidance in natural herbaceous populations. Plant Sci. 234, 155–162 (2015).

33. D. H. Valentine, J. Clausen, H. Clausen, M. William, Experimental studies on the nature of species. IV. Genetic structure of ecological races. J. Ecol. 47, 707 (1959).

34. G. L. Stebbins Jr, Aridity as a stimulus to plant evolution. Am. Nat. 86, 33–44 (1952).

35. X. Yu, et al., Morphological structure and physiological and biochemical responses to drought stress of Iris japonica. Plants 12 (2023).

36. S. Tiwari, C. Lata, P. S. Chauhan, V. Prasad, M. Prasad, A functional genomic perspective on drought signalling and its crosstalk with phytohormone-mediated signalling pathways in plants. Curr. Genomics 18, 469–482 (2017).

37. M. Pfenninger, et al., Genomic basis for drought resistance in European beech forests threatened

by climate change. Elife 10 (2021).

38. M. Nyine, et al., Genomic signals of ecogeographic adaptation in a wild relative are associated with improved wheat performance under drought stress. Genome Biol. 26, 35 (2025).

39. W. A. Lopez-Arboleda, S. Reinert, M. Nordborg, A. Korte, Global genetic heterogeneity in adaptive traits. Mol. Biol. Evol. 38, 4822–4831 (2021).

40. M. Mayrose, N. C. Kane, I. Mayrose, K. M. Dlugosch, L. H. Rieseberg, Increased growth in sunflower correlates with reduced defences and altered gene expression in response to biotic and abiotic stress. Mol. Ecol. 20, 4683–4694 (2011).

41. P. E. Verslues, M. Agarwal, S. Katiyar-Agarwal, J. Zhu, J.-K. Zhu, Methods and concepts in quantifying resistance to drought, salt and freezing, abiotic stresses that affect plant water status. Plant J. 45, 523–539 (2006).

42. K. E. Waselkov, N. D. Regenold, R. C. Lum, K. M. Olsen, Agricultural adaptation in the native North American weed waterhemp, Amaranthus tuberculatus (Amaranthaceae). PLoS One 15, e0238861 (2020).

43. J. Sauer, Recent migration and evolution of the dioecious amaranths. Evolution 11, 11–31 (1957).

44. J. M. Kreiner, A. Caballero, S. I. Wright, J. R. Stinchcombe, Selective ancestral sorting and de novo evolution in the agricultural invasion of Amaranthus tuberculatus. Evolution (2021). https://doi.org/10.1111/evo.14404.

45. M. Costea, S. E. Weaver, F. J. Tardif, The Biology of Invasive Alien Plants in Canada. 3. Amaranthus tuberculatus (Moq.) Sauer var. rudis (Sauer) Costea & Tardif. Can. J. Plant Sci. 85, 507–522 (2005).

46. J. M. Kreiner, et al., Multiple modes of convergent adaptation in the spread of glyphosate-resistant Amaranthus tuberculatus. Proc. Natl. Acad. Sci. U. S. A. 116, 21076–21084 (2019).

47. S. R. Keller, D. R. Taylor, History, chance and adaptation during biological invasion: separating stochastic phenotypic evolution from response to selection. Ecol. Lett. 11, 852–866 (2008).

48. H. M. Cockerton, et al., Fitness cost associated with enhanced EPSPS gene copy number and glyphosate resistance in an Amaranthus tuberculatus population. Cold Spring Harbor Laboratory 2021.01.09.426028 (2021).

49. D. H. Alexander, J. Novembre, K. Lange, Fast model-based estimation of ancestry in unrelated individuals. Genome Res. 19, 1655–1664 (2009).

50. J. Marchini, L. R. Cardon, M. S. Phillips, P. Donnelly, The effects of human population structure on large genetic association studies. Nat. Genet. 36, 512–517 (2004).

51. M. L. Freedman, et al., Assessing the impact of population stratification on genetic association studies. Nat. Genet. 36, 388–393 (2004).

52. L. Bresadola, et al., Admixture mapping in interspecific Populus hybrids identifies classes of genomic architectures for phytochemical, morphological and growth traits. New Phytol. 223, 2076–2089 (2019).

53. P. M. McKeigue, Prospects for admixture mapping of complex traits. Am. J. Hum. Genet. 76, 1–7 (2005).

54. N. V. Robles, et al., Admixture mapping reveals evidence for multiple mitonuclear incompatibilities in swordtail fish hybrids. Evolutionary Biology (2025).

55. R. Corbett-Detig, R. Nielsen, A hidden Markov model approach for simultaneously estimating local ancestry and admixture time using next generation sequence data in samples of arbitrary ploidy. PLoS Genet. 13, e1006529 (2017).

56. T. Ivanova, I. Dincheva, I. Badjakov, A. Iantcheva, Transcriptional and metabolic profiling of Arabidopsis thaliana transgenic plants expressing histone acetyltransferase HAC1 upon the application of abiotic stress-salt and low temperature. Metabolites 13 (2023).

57. V. González-Mendoza, et al., APSR1, a novel gene required for meristem maintenance, is negatively regulated by low phosphate availability. Plant Sci. 205-206, 2–12 (2013).

58. Y.-Y. Wang, D. J. Head, B. A. Hauser, During water stress, fertility modulated by ROS scavengers abundant in Arabidopsis pistils. Plants 12 (2023).

59. C. Lin, et al., Genome-wide survey of the RWP-RK gene family in cassava (Manihot esculenta crantz) and functional analysis. Int. J. Mol. Sci. 24, 12925 (2023).

60. A. Valletta, L. Trainotti, A. R. Santamaria, G. Pasqua, Cell-specific expression of tryptophan decarboxylase and 10-hydroxygeraniol oxidoreductase, key genes involved in camptothecin biosynthesis in Camptotheca acuminata Decne (Nyssaceae). BMC Plant Biol. 10, 69 (2010).

61. Y. Lian, et al., SUPPRESSOR OF MAX2 LIKE 6, 7, and 8 interact with DDB1 BINDING WD REPEAT DOMAIN HYPERSENSITIVE TO ABA DEFICIENT 1 to regulate the drought tolerance and target SUCROSE NONFERMENTING 1 RELATED PROTEIN KINASE 2.3 to abscisic acid response in Arabidopsis. Biomolecules 13, 1406 (2023).

62. J.-H. Lee, W. Terzaghi, X. W. Deng, DWA3, an Arabidopsis DWD protein, acts as a negative regulator in ABA signal transduction. Plant Sci. 180, 352–357 (2011).

63. M. Miao, et al., The tomato DWD motif-containing protein DDI1 interacts with the CUL4-DDB1-based ubiquitin ligase and plays a pivotal role in abiotic stress responses. Biochem. Biophys. Res. Commun. 450, 1439–1445 (2014).

64. N. R. Wray, M. E. Goddard, P. M. Visscher, Prediction of individual genetic risk to disease from genome-wide association studies. Genome Res. 17, 1520–1528 (2007).

65. A. Dai, Increasing drought under global warming in observations and models. Nat. Clim. Chang. 3, 52–58 (2013).

66. N. Barghi, J. Hermisson, C. Schlötterer, Polygenic adaptation: a unifying framework to understand positive selection. Nat. Rev. Genet. 21, 769–781 (2020).

67. K. Kosheleva, M. M. Desai, Recombination alters the dynamics of adaptation on standing variation in laboratory yeast populations. Mol. Biol. Evol. 35, 180–201 (2018).

68. M. C. Turchin, et al., Evidence of widespread selection on standing variation in Europe at height-associated SNPs. Nat. Genet. 44, 1015–1019 (2012).

69. M. G. Stetter, K. Thornton, J. Ross-Ibarra, Genetic architecture and selective sweeps after polygenic adaptation to distant trait optima. PLoS Genet. 14, e1007794 (2018).

70. S. Matuszewski, J. Hermisson, M. Kopp, Catch me if you can: Adaptation from standing genetic variation to a moving phenotypic optimum. Genetics 200, 1255–1274 (2015).

71. M. Sohail, et al., Polygenic adaptation on height is overestimated due to uncorrected stratification in genome-wide association studies. Elife 8 (2019).

72. K. C. Fetter, S. R. Keller, Admixture mapping and selection scans identify genomic regions associated with stomatal patterning and disease resistance in hybrid poplars. Ecol. Evol. 13, e10579 (2023).

73. D. Shriner, Overview of admixture mapping. Curr. Protoc. 3, e677 (2023).

74. J. M. Kreiner, J. R. Stinchcombe, S. I. Wright, Population genomics of herbicide resistance: Adaptation via evolutionary rescue. Annu. Rev. Plant Biol. 69, 611–635 (2018).

75. J. M. Kreiner, et al., Repeated origins, widespread gene flow, and allelic interactions of target-site herbicide resistance mutations. Elife 11, e70242 (2022).

76. J. M. Valliere, Tradeoffs between growth rate and water-use efficiency in seedlings of native perennials but not invasive annuals. Plant Ecol. 220, 361–369 (2019).

77. L. Koziol, L. H. Rieseberg, N. Kane, J. D. Bever, Reduced drought tolerance during domestication and the evolution of weediness results from tolerance-growth trade-offs. Evolution 66, 3803–3814 (2012).

78. B. E. Goulet-Scott, et al., A multidimensional selective landscape drives adaptive divergence between and within closely related Phlox species. Nat. Commun. 15, 4661 (2024).

79. J. Antonovics, R. B. Primack, Experimental ecological genetics in Plantago. VI. The demography of seed- ling transplants of P. lanceolata. J. Ecol 70, 55–75 (1982).

80. D. A. Levin, Consequences of stochastic elements in plant migration. Am. Nat. 132, 643–651 (1988).

81. T. F. Hansen, Three modes of evolution? Remarks on rates of evolution and time scaling. J. Evol. Biol. 37, 1523–1537 (2024).

82. S. C. Groen, et al., The strength and pattern of natural selection on gene expression in rice. Nature 578, 572–576 (2020).

83. I. Ćalić, et al., The influence of genetic architecture on responses to selection under drought in rice. Evol. Appl. 15, 1670–1690 (2022).

84. C. Carvalho, et al., Multivariate selection mediated by aridity predicts divergence of drought-resistant traits along natural aridity gradients of an invasive weed. New Phytol. 234, 1088–1100 (2022).

85. B. T. Hendrickson, et al., Evolution of drought resistance strategies following the introduction of white clover (Trifolium repens L.). Ann. Bot. (2025). https://doi.org/10.1093/aob/mcaf037.

86. D. B. Lowry, et al., The genetics of divergence and reproductive isolation between ecotypes of Panicum hallii. New Phytol. 205, 402–414 (2015).

87. M. Sinclair-Waters, et al., Beyond large-effect loci: large-scale GWAS reveals a mixed large-effect and polygenic architecture for age at maturity of Atlantic salmon. Genet. Sel. Evol. 52, 9 (2020).

88. M. Exposito-Alonso, A. C. Brennan, C. Alonso-Blanco, F. X. Picó, Spatio-temporal variation in fitness responses to contrasting environments in Arabidopsis thaliana. Evolution (2018). https://doi.org/10.1111/evo.13508.

89. D. Tataru, E. C. Wheeler, K. G. Ferris, Spatially and temporally varying selection influence species boundaries in two sympatric Mimulus. Proc. Biol. Sci. 290, 20222279 (2023).

90. S. N. Sheth, et al., Evolutionary responses to historic drought across the range of scarlet monkeyflower. bioRxiv 2025.05.20.655098 (2025).

91. R. Rauschkolb, et al., Evolution of plant drought strategies and herbivore tolerance after two decades of climate change. New Phytol. 235, 773–785 (2022).

92. L. M. Bono, L. B. Smith Jr, D. W. Pfennig, C. L. Burch, The emergence of performance trade-offs during local adaptation: insights from experimental evolution. Mol. Ecol. 26, 1720–1733 (2017).

93. N. J. Kooyers, et al., Lagging Adaptation to Climate Supersedes Local Adaptation to Herbivory in an Annual Monkeyflower. Am. Nat. 194, 541–557 (2019).

94. G. M. Walter, et al., Local adaptation in climate tolerance at a small geographic scale contrasts with broad latitudinal patterns. bioRxiv 2025.05.27.655235 (2025).

95. J. T. Anderson, C.-R. Lee, T. Mitchell-Olds, Strong selection genome-wide enhances fitness trade-offs across environments and episodes of selection: Special section. Evolution 68, 16–31 (2014).

96. H. Sato, J. Mizoi, K. Shinozaki, K. Yamaguchi-Shinozaki, Complex plant responses to drought and heat stress under climate change. Plant J. 117, 1873–1892 (2024).

97. T. Tang, et al., Drought frequency, intensity, and exposure have increased due to historical land use and land cover changes. Commun. Earth Environ. 6, 1–13 (2025).

98. M. M. Ludlow, Structural and Functional Responses to Environmental Stresses, K. H. Kreeeb, H. Richter, T. M. Hinckley, Eds. (SPB Academic Publishing, 1989).

99. S. J. Franks, Plasticity and evolution in drought avoidance and escape in the annual plant Brassica rapa. New Phytol. 190, 249–257 (2011).

100. J. Zeng, Y. P. Zou, J. Y. Bai, H. S. Zheng, Preparation of total DNA from “recalcitrant plant taxa.” Acta Botanica Sinica 44, 694–697 (2002).

101. M. G. Murray, W. F. Thompson, Rapid isolation of high molecular weight plant DNA. Nucleic Acids Res. 8, 4321–4325 (1980).

102. B. A. Rowan, V. Patel, D. Weigel, K. Schneeberger, Rapid and inexpensive whole-genome genotyping-by-sequencing for crossover localization and fine-scale genetic mapping. G3 (Bethesda) 5, 385–398 (2015).

103. N. Rohland, D. Reich, Cost-effective, high-throughput DNA sequencing libraries for multiplexed target capture. Genome Res. 22, 939–946 (2012).

104. J. M. Kreiner, et al., The evolution of separate sexes in waterhemp is associated with surprising chromosomal diversity and complexity. PLoS Biol. 23, e3003254 (2025).

105. S. Purcell, et al., PLINK: a tool set for whole-genome association and population-based linkage analyses. Am. J. Hum. Genet. 81, 559–575 (2007).

106. J. Svedberg, 1vladimir Shchur, S. Reinman, R. Nielsen, R. Corbett-Detig, Inferring adaptive introgression using hidden Markov models. Evol. Conserv. Biodivers. 38, 2152–2165.

107. X. Zhou, M. Stephens, Genome-wide efficient mixed-model analysis for association studies. Nat. Genet. 44, 821–824 (2012).

108. H. Mi, et al., The PANTHER database of protein families, subfamilies, functions and pathways. Nucleic Acids Res. 33, D284–8 (2005).

109. J. J. Berg, G. Coop, A population genetic signal of polygenic adaptation. PLoS Genet. 10, e1004412 (2014).

1. P. W. Messer, S. P. Ellner, N. G. Hairston Jr, Can Population Genetics Adapt to Rapid Evolution? *Trends Genet.* **32**, 408–418 (2016).

2. S. Yeaman, Evolution of polygenic traits under global vs local adaptation. *Genetics* **220** (2022).

3. J. T. Stroud, M. P. Moore, R. B. Langerhans, J. B. Losos, Fluctuating selection maintains distinct species phenotypes in an ecological community in the wild. *Proc. Natl. Acad. Sci. U. S. A.* **120**, e2222071120 (2023).

4. S. Yeaman, M. C. Whitlock, The genetic architecture of adaptation under migration-selection balance. *Evolution* **65**, 1897–1911 (2011).

5. J. B. S. Haldane, A mathematical theory of natural and artificial selection. *Math. Proc. Camb. Philos. Soc.* **23**, 363–372 (1926).

6. R. D. H. Barrett, D. Schluter, Adaptation from standing genetic variation. *Trends Ecol. Evol.* **23**, 38–44 (2008).

7. J. M. Cocciardi, *et al.*, The value of long-term ecological research for evolutionary insights. *Nat. Ecol. Evol.* **8**, 1584–1592 (2024).

8. K. E. Brown, D. Koenig, On the hidden temporal dynamics of plant adaptation. *Curr. Opin. Plant Biol.* **70**, 102298 (2022).

9. J. M. Kreiner, The genetic architecture and spatiotemporal dynamics of adaptation across human-modified landscapes. *New Phytol.* (2025). https://doi.org/10.1111/nph.70520.

10. S. Busoms, *et al.*, Fluctuating selection on migrant adaptive sodium transporter alleles in coastal Arabidopsis thaliana. *Proc. Natl. Acad. Sci. U. S. A.* **115**, E12443–E12452 (2018).

11. A. O. Bergland, E. L. Behrman, K. R. O'Brien, P. S. Schmidt, D. A. Petrov, Genomic evidence of rapid and stable adaptive oscillations over seasonal time scales in Drosophila. *PLoS Genet.* **10**, e1004775 (2014).

12. J. K. Kelly, The genomic scale of fluctuating selection in a natural plant population. *Evolution Letters* **n/a** (2022).

13. S. M. Rudman, *et al.*, Direct observation of adaptive tracking on ecological time scales in *Drosophila*. *Science* **375**, eabj7484 (2022).

14. M. C. Bitter, *et al.*, Continuously fluctuating selection reveals fine granularity of adaptation. *Nature* **634**, 389–396 (2024).

15. A. Troth, J. R. Puzey, R. S. Kim, J. H. Willis, J. K. Kelly, Selective trade-offs maintain alleles underpinning complex trait variation in plants. *Science* **361**, 475–478 (2018).

16. H. A. Burbano, R. M. Gutaker, Ancient DNA genomics and the renaissance of herbaria. *Science* **382**, 59–63 (2023).

17. L. Eckert, I. Eckert, O. Rahn, C. P. So, R. D. H. Barrett, Using herbarium collections to study genetic responses to global change. *New Phytol.* (2025). https://doi.org/10.1111/nph.70454.

18. A. S. Kim, *et al.*, Temporal collections to study invasion biology. *Mol. Ecol.* (2023). https://doi.org/10.1111/mec.17176.

19. J. M. Kreiner, *et al.*, Rapid weed adaptation and range expansion in response to agriculture over the past two centuries. *Science* **378**, 1079–1085 (2022).

20. P. L. M. Lang, *et al.*, Century-long timelines of herbarium genomes predict plant stomatal response to climate change. *Nat. Ecol. Evol.* **8**, 1641–1653 (2024).

21. P. Battlay, *et al.*, Large haploblocks underlie rapid adaptation in the invasive weed Ambrosia artemisiifolia. *Nat. Commun.* **14**, 1717 (2023).

22. O. L. Johnson, R. Tobler, J. M. Schmidt, C. D. Huber, Fluctuating selection and the determinants of genetic variation. *Trends Genet.* **39**, 491–504 (2023).

23. G. Bell, S. Collins, Adaptation, extinction and global change: Adaption, extinction and global change. *Evol. Appl.* **1**, 3–16 (2008).

24. A. K. Mishra, V. P. Singh, A review of drought concepts. *J. Hydrol. (Amst.)* **391**, 202–216 (2010).

25. A. M. Siepielski, *et al.*, Precipitation drives global variation in natural selection. *Science* **355**, 959–962 (2017).

26. R. E. Kramp, *et al.*, Functional traits and their plasticity shift from tolerant to avoidant under extreme drought. *Ecology* **103**, e3826 (2022).

27. N. J. Kooyers, The evolution of drought escape and avoidance in natural herbaceous populations. *Plant Sci.* **234**, 155–162 (2015).

28. D. H. Valentine, J. Clausen, H. Clausen, M. William, Experimental studies on the nature of species. IV. Genetic structure of ecological races. *J. Ecol.* **47**, 707 (1959).

29. G. L. Stebbins Jr, Aridity as a stimulus to plant evolution. *Am. Nat.* **86**, 33–44 (1952).

30. X. Yu, *et al.*, Morphological structure and physiological and biochemical responses to drought stress of Iris japonica. *Plants* **12** (2023).

31. S. Tiwari, C. Lata, P. S. Chauhan, V. Prasad, M. Prasad, A functional genomic

perspective on drought signalling and its crosstalk with phytohormone-mediated signalling pathways in plants. *Curr. Genomics* **18**, 469–482 (2017).

32. M. Exposito-Alonso, *et al.*, Genomic basis and evolutionary potential for extreme drought adaptation in Arabidopsis thaliana. *Nat. Ecol. Evol.* **2**, 352–358 (2018).

33. M. Pfenninger, *et al.*, Genomic basis for drought resistance in European beech forests threatened by climate change. *Elife* **10** (2021).

34. M. Nyine, *et al.*, Genomic signals of ecogeographic adaptation in a wild relative are associated with improved wheat performance under drought stress. *Genome Biol.* **26**, 35 (2025).

35. W. A. Lopez-Arboleda, S. Reinert, M. Nordborg, A. Korte, Global genetic heterogeneity in adaptive traits. *Mol. Biol. Evol.* **38**, 4822–4831 (2021).

36. M. Mayrose, N. C. Kane, I. Mayrose, K. M. Dlugosch, L. H. Rieseberg, Increased growth in sunflower correlates with reduced defences and altered gene expression in response to biotic and abiotic stress. *Mol. Ecol.* **20**, 4683–4694 (2011).

37. P. E. Verslues, M. Agarwal, S. Katiyar-Agarwal, J. Zhu, J.-K. Zhu, Methods and concepts in quantifying resistance to drought, salt and freezing, abiotic stresses that affect plant water status. *Plant J.* **45**, 523–539 (2006).

38. K. E. Waselkov, N. D. Regenold, R. C. Lum, K. M. Olsen, Agricultural adaptation in the native North American weed waterhemp, Amaranthus tuberculatus (Amaranthaceae). *PLoS One* **15**, e0238861 (2020).

39. J. Sauer, Recent migration and evolution of the dioecious amaranths. *Evolution* **11**, 11–31 (1957).

40. J. M. Kreiner, A. Caballero, S. I. Wright, J. R. Stinchcombe, Selective ancestral sorting and de novo evolution in the agricultural invasion of Amaranthus tuberculatus. *Evolution* (2021). https://doi.org/10.1111/evo.14404.

41. M. Costea, S. E. Weaver, F. J. Tardif, The Biology of Invasive Alien Plants in Canada. 3. Amaranthus tuberculatus (Moq.) Sauer var. rudis (Sauer) Costea & Tardif. *Can. J. Plant Sci.* **85**, 507–522 (2005).

42. S. R. Keller, D. R. Taylor, History, chance and adaptation during biological invasion: separating stochastic phenotypic evolution from response to selection. *Ecol. Lett.* **11**, 852–866 (2008).

43. H. M. Cockerton, *et al.*, Fitness cost associated with enhanced EPSPS gene copy number and glyphosate resistance in an Amaranthus tuberculatus population. *Cold Spring Harbor Laboratory* 2021.01.09.426028 (2021).

44. D. H. Alexander, J. Novembre, K. Lange, Fast model-based estimation of ancestry in unrelated individuals. *Genome Res.* **19**, 1655–1664 (2009).

45. R. Corbett-Detig, R. Nielsen, A hidden Markov model approach for simultaneously estimating local ancestry and admixture time using next generation sequence data in

samples of arbitrary ploidy. *PLoS Genet.* **13**, e1006529 (2017).

46. T. Ivanova, I. Dincheva, I. Badjakov, A. Iantcheva, Transcriptional and metabolic profiling of Arabidopsis thaliana transgenic plants expressing histone acetyltransferase HAC1 upon the application of abiotic stress-salt and low temperature. *Metabolites* **13** (2023).

47. V. González-Mendoza, *et al.*, APSR1, a novel gene required for meristem maintenance, is negatively regulated by low phosphate availability. *Plant Sci.* **205-206**, 2–12 (2013).

48. Y.-Y. Wang, D. J. Head, B. A. Hauser, During water stress, fertility modulated by ROS scavengers abundant in Arabidopsis pistils. *Plants* **12** (2023).

49. C. Lin, *et al.*, Genome-wide survey of the RWP-RK gene family in cassava (Manihot esculenta crantz) and functional analysis. *Int. J. Mol. Sci.* **24**, 12925 (2023).

50. A. Valletta, L. Trainotti, A. R. Santamaria, G. Pasqua, Cell-specific expression of tryptophan decarboxylase and 10-hydroxygeraniol oxidoreductase, key genes involved in camptothecin biosynthesis in Camptotheca acuminata Decne (Nyssaceae). *BMC Plant Biol.* **10**, 69 (2010).

51. Y. Lian, *et al.*, SUPPRESSOR OF MAX2 LIKE 6, 7, and 8 interact with DDB1 BINDING WD REPEAT DOMAIN HYPERSENSITIVE TO ABA DEFICIENT 1 to regulate the drought tolerance and target SUCROSE NONFERMENTING 1 RELATED PROTEIN KINASE 2.3 to abscisic acid response in Arabidopsis. *Biomolecules* **13**, 1406 (2023).

52. J.-H. Lee, W. Terzaghi, X. W. Deng, DWA3, an Arabidopsis DWD protein, acts as a negative regulator in ABA signal transduction. *Plant Sci.* **180**, 352–357 (2011).

53. M. Miao, *et al.*, The tomato DWD motif-containing protein DDI1 interacts with the CUL4-DDB1-based ubiquitin ligase and plays a pivotal role in abiotic stress responses. *Biochem. Biophys. Res. Commun.* **450**, 1439–1445 (2014).

54. N. R. Wray, M. E. Goddard, P. M. Visscher, Prediction of individual genetic risk to disease from genome-wide association studies. *Genome Res.* **17**, 1520–1528 (2007).

55. A. Dai, Increasing drought under global warming in observations and models. *Nat. Clim. Chang.* **3**, 52–58 (2013).

56. N. Barghi, J. Hermisson, C. Schlötterer, Polygenic adaptation: a unifying framework to understand positive selection. *Nat. Rev. Genet.* **21**, 769–781 (2020).

57. K. Kosheleva, M. M. Desai, Recombination alters the dynamics of adaptation on standing variation in laboratory yeast populations. *Mol. Biol. Evol.* **35**, 180–201 (2018).

58. M. C. Turchin, *et al.*, Evidence of widespread selection on standing variation in Europe at height-associated SNPs. *Nat. Genet.* **44**, 1015–1019 (2012).

59. M. G. Stetter, K. Thornton, J. Ross-Ibarra, Genetic architecture and selective sweeps after polygenic adaptation to distant trait optima. *PLoS Genet.* **14**, e1007794 (2018).

60. S. Matuszewski, J. Hermisson, M. Kopp, Catch me if you can: Adaptation from standing genetic variation to a moving phenotypic optimum. *Genetics* **200**, 1255–1274 (2015).

61. M. Sohail, *et al.*, Polygenic adaptation on height is overestimated due to uncorrected stratification in genome-wide association studies. *Elife* **8** (2019).

62. J. M. Kreiner, J. R. Stinchcombe, S. I. Wright, Population genomics of herbicide resistance: Adaptation via evolutionary rescue. *Annu. Rev. Plant Biol.* **69**, 611–635 (2018).

63. J. M. Kreiner, *et al.*, Repeated origins, widespread gene flow, and allelic interactions of target-site herbicide resistance mutations. *Elife* **11**, e70242 (2022).

64. J. M. Valliere, Tradeoffs between growth rate and water-use efficiency in seedlings of native perennials but not invasive annuals. *Plant Ecol.* **220**, 361–369 (2019).

65. L. Koziol, L. H. Rieseberg, N. Kane, J. D. Bever, Reduced drought tolerance during domestication and the evolution of weediness results from tolerance-growth trade-offs. *Evolution* **66**, 3803–3814 (2012).

66. B. E. Goulet-Scott, *et al.*, A multidimensional selective landscape drives adaptive divergence between and within closely related Phlox species. *Nat. Commun.* **15**, 4661 (2024).

67. J. Antonovics, R. B. Primack, Experimental ecological genetics in Plantago. VI. The demography of seed- ling transplants of P. lanceolata. *J. Ecol* **70**, 55–75 (1982).

68. D. A. Levin, Consequences of stochastic elements in plant migration. *Am. Nat.* **132**, 643–651 (1988).

69. R. Gargiulo, K. B. Budde, M. Heuertz, Mind the lag: understanding genetic extinction debt for conservation. *Trends Ecol. Evol.* **40**, 228–237 (2025).

70. T. F. Hansen, Three modes of evolution? Remarks on rates of evolution and time scaling. *J. Evol. Biol.* **37**, 1523–1537 (2024).

71. B. T. Hendrickson, *et al.*, Evolution of drought resistance strategies following the introduction of white clover (Trifolium repens L.). *Ann. Bot.* (2025). https://doi.org/10.1093/aob/mcaf037.

72. D. B. Lowry, *et al.*, The genetics of divergence and reproductive isolation between ecotypes of Panicum hallii. *New Phytol.* **205**, 402–414 (2015).

73. A. F. Elfarargi, *et al.*, Dissecting the genetic basis of drought escape across multiple traits in colonizing Arabidopsis thaliana lineages. *bioRxiv* (2025).

74. H. De Kort, *et al.*, Signatures of polygenic adaptation align with genome-wide methylation patterns in wild strawberry plants. *New Phytol.* **235**, 1501–1514 (2022).

75. A. F. Elfarargi, *et al.*, Dissecting the genetic basis of drought escape across multiple traits in colonizing *Arabidopsis thaliana* lineages. *bioRxiv* 2025.04.07.647068 (2025).

76. M. Sinclair-Waters, *et al.*, Beyond large-effect loci: large-scale GWAS reveals a mixed large-effect and polygenic architecture for age at maturity of Atlantic salmon. *Genet. Sel. Evol.* **52**, 9 (2020).

77. J. K. McKay, J. H. Richards, T. Mitchell-Olds, Genetics of drought adaptation in Arabidopsis thaliana: I. Pleiotropy contributes to genetic correlations among ecological traits. *Mol. Ecol.* **12**, 1137–1151 (2003).

78. W. Zegada-Lizarazu, Y. Izumi, M. Iijima, Water competition of intercropped pearl millet with cowpeaunder drought and soil compaction stresses. *Plant Prod. Sci.* **9**, 123–132 (2006).

79. M. A. Hamza, W. K. Anderson, Soil compaction in cropping systems. *Soil Tillage Res.* **82**, 121–145 (2005).

80. K. R. Robertson, The genera of Amaranthaceae in the southeastern United States. *Journal of the Arnold Arboretum* **62**, 267–313 (1981).

81. J. Zeng, Y. P. Zou, J. Y. Bai, H. S. Zheng, Preparation of total DNA from "recalcitrant plant taxa." *Acta Botanica Sinica* **44**, 694–697 (2002).

82. M. G. Murray, W. F. Thompson, Rapid isolation of high molecular weight plant DNA. *Nucleic Acids Res.* **8**, 4321–4325 (1980).

83. B. A. Rowan, V. Patel, D. Weigel, K. Schneeberger, Rapid and inexpensive whole-genome genotyping-by-sequencing for crossover localization and fine-scale genetic mapping. *G3 (Bethesda)* **5**, 385–398 (2015).

84. N. Rohland, D. Reich, Cost-effective, high-throughput DNA sequencing libraries for multiplexed target capture. *Genome Res.* **22**, 939–946 (2012).

85. J. M. Kreiner, *et al.*, The evolution of separate sexes in waterhemp is associated with surprising chromosomal diversity and complexity. *PLoS Biol.* **23**, e3003254 (2025).

86. H. Jónsson, A. Ginolhac, M. Schubert, P. L. F. Johnson, L. Orlando, mapDamage2.0: fast approximate Bayesian estimates of ancient DNA damage parameters. *Bioinformatics* **29**, 1682–1684 (2013).

87. A. Peltzer, *et al.*, EAGER: efficient ancient genome reconstruction. *Genome Biol.* **17**, 60 (2016).

88. J. M. Kreiner, *et al.*, Multiple modes of convergent adaptation in the spread of glyphosate-resistant *Amaranthus tuberculatus*. *Proc. Natl. Acad. Sci. U. S. A.* **116**, 21076–21084 (2019).

89. B. S. Pedersen, A. R. Quinlan, Mosdepth: quick coverage calculation for genomes and exomes. *Bioinformatics* **34**, 867–868 (2018).

90. S. Purcell, *et al.*, PLINK: a tool set for whole-genome association and population-based linkage analyses. *Am. J. Hum. Genet.* **81**, 559–575 (2007).

91. J. Svedberg, 1vladimir Shchur, S. Reinman, R. Nielsen, R. Corbett-Detig, Inferring

adaptive introgression using hidden Markov models. *Evol. Conserv. Biodivers.* **38**, 2152–2165.

92. J. J. Berg, G. Coop, A population genetic signal of polygenic adaptation. *PLoS Genet.* **10**, e1004412 (2014).

93. D. M. Emms, S. Kelly, OrthoFinder2: fast and accurate phylogenomic orthology analysis from gene sequences. *BioRxiv* **466201** (2018).

94. H. Mi, *et al.*, The PANTHER database of protein families, subfamilies, functions and pathways. *Nucleic Acids Res.* **33**, D284–8 (2005).

95. P. Cingolani, *et al.*, A program for annotating and predicting the effects of single nucleotide polymorphisms, SnpEff: SNPs in the genome of Drosophila melanogaster strain w1118; iso-2; iso-3. *Fly (Austin)* **6**, 80–92 (2012).

Supplementary Materials for Pineau et al., 2025

Supplementary Figures

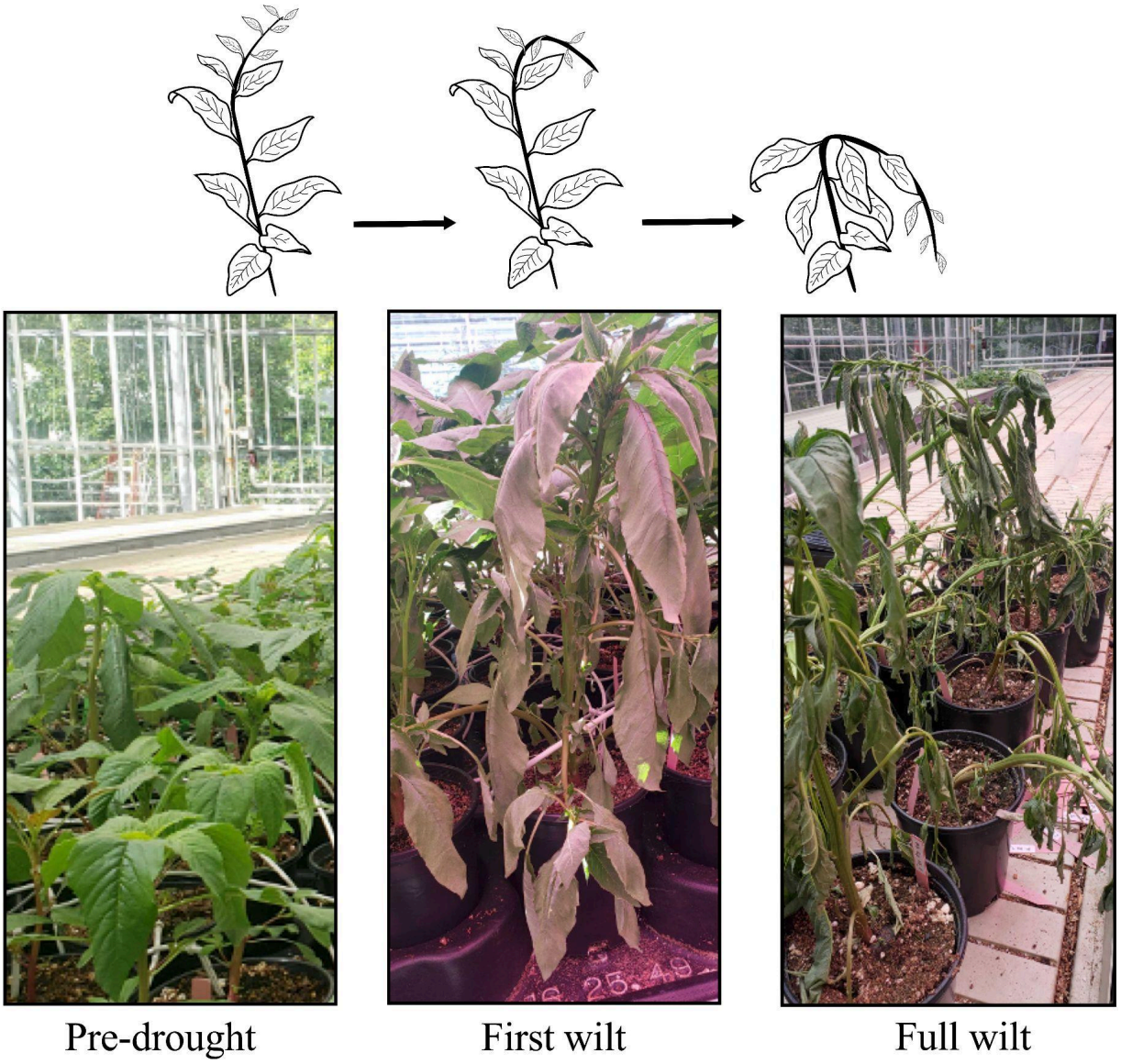

Fig. S1. Plant survival under drought conditions was monitored every day during 20 days (until all drought-treated plants had died). The day at which the first signs of substantial leaf wilt were observed was labeled as "first wilt". The day to "full wilt" corresponds to complete loss of turgor pressure throughout the plant.

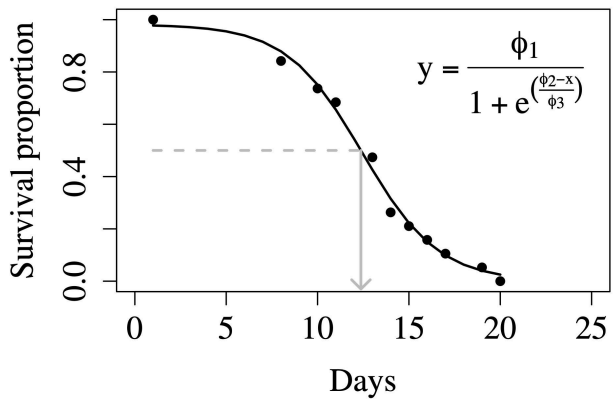

Fig. S2. A logistic model was fitted to the survival curves using *nls* and *SSlogit* in R. The parameters estimated from the fit were then used to calculate LD_{50}, the day at which half of the population has died.

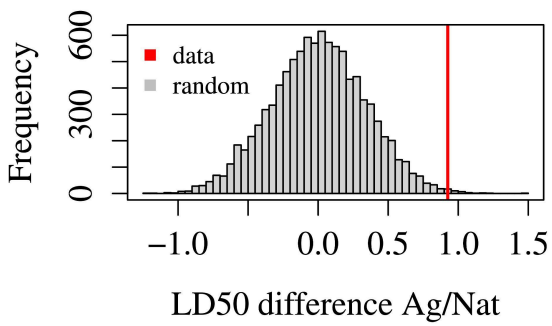

Fig. S3. Populations in agricultural habitats are significantly more resilient to drought as compared to those from natural habitats. We permuted 10,000 times the population assignment for their habitat, and calculated the difference between the mean LD_{50} value in agricultural versus natural habitats (gray distribution). The mean value for the data is shown in red (p-value = 0.0036).

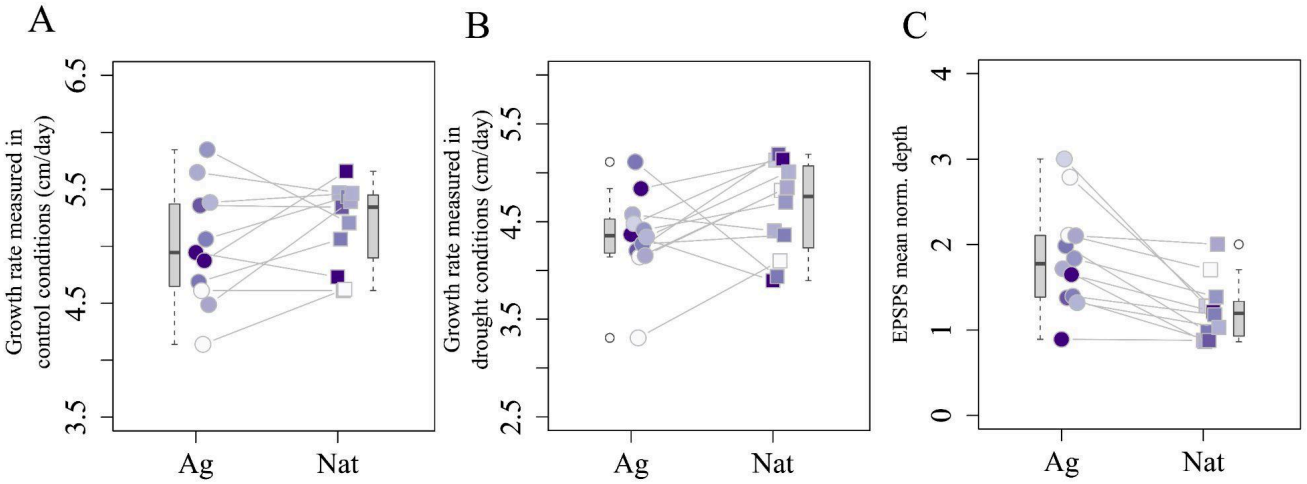

Fig. S4. Mean growth rate in control (A) and drought (B) conditions per population, and EPSPS mean normalized copy number per population (C), compared between environments (Ag/NAt). Wilcoxon paired test for growth rate in drought conditions, p-value = 0.06; Wilcoxon paired test for growth rate in control conditions, p-value = 0.89; Wilcoxon paired test for EPSPS mean normalized depth, p-value = 0.00024.

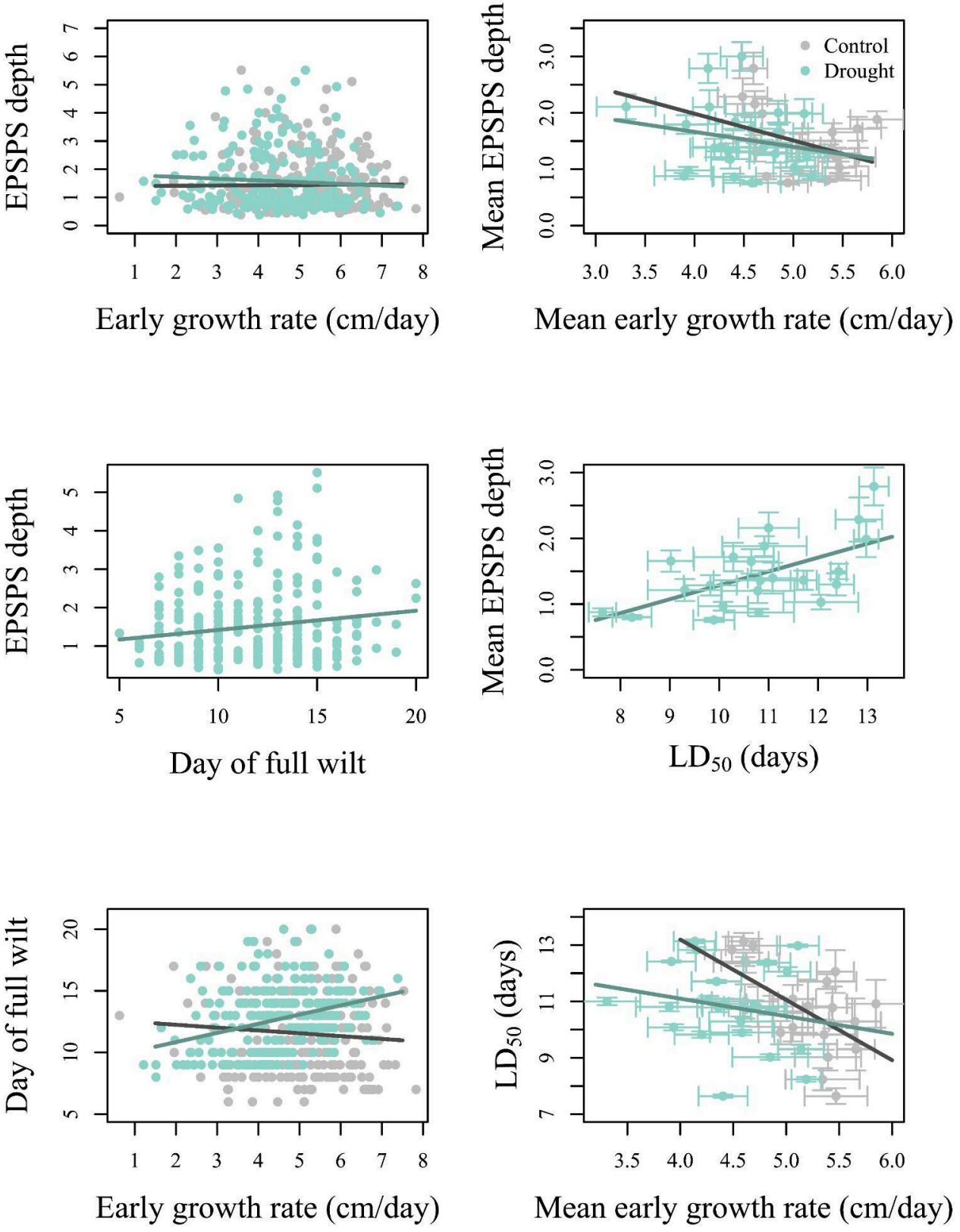

Fig. S5. Individual-level trade-offs (left) and population-level trade-offs (right) between growth, resistance to drought (day to full wilt and LD_{50}) and resistance to herbicide (EPSPS copy number). The growth rate was measured in both control (gray) and drought treated (teal) individuals. To look at the effect of drought on growth versus survival, we match the survival values (day to full wilt and LD_{50}) of the treated plants to their half sibling counterparts.

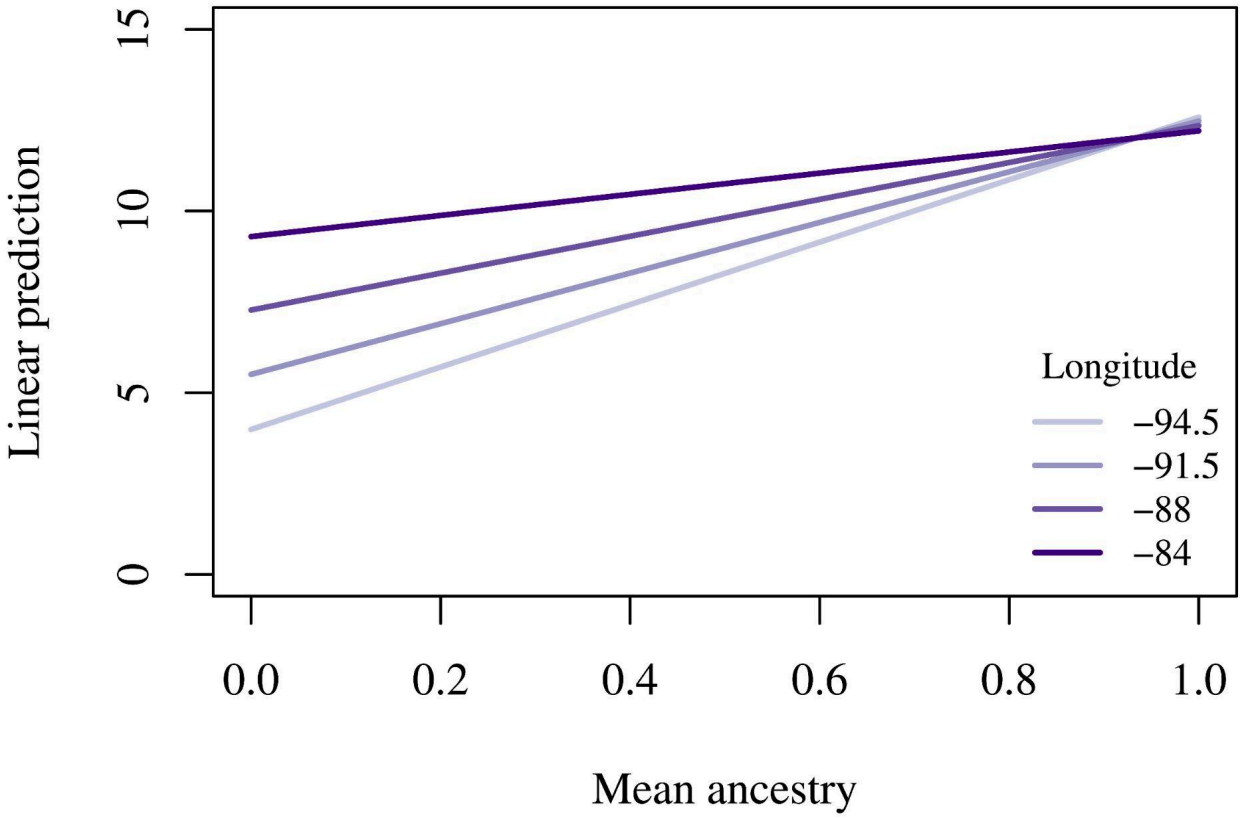

Fig. S6. Linear predictions of drought resistance (LD_{50}, in days) of the effect of admixture and longitude from a multivariate model. The combined effects of admixture and longitude were averaged over the habitats (natural and agricultural). Predictions in drought response depend on the interaction between geography and ancestry, with pure var. *rudis* ancestry being always advantageous independent of the longitude.

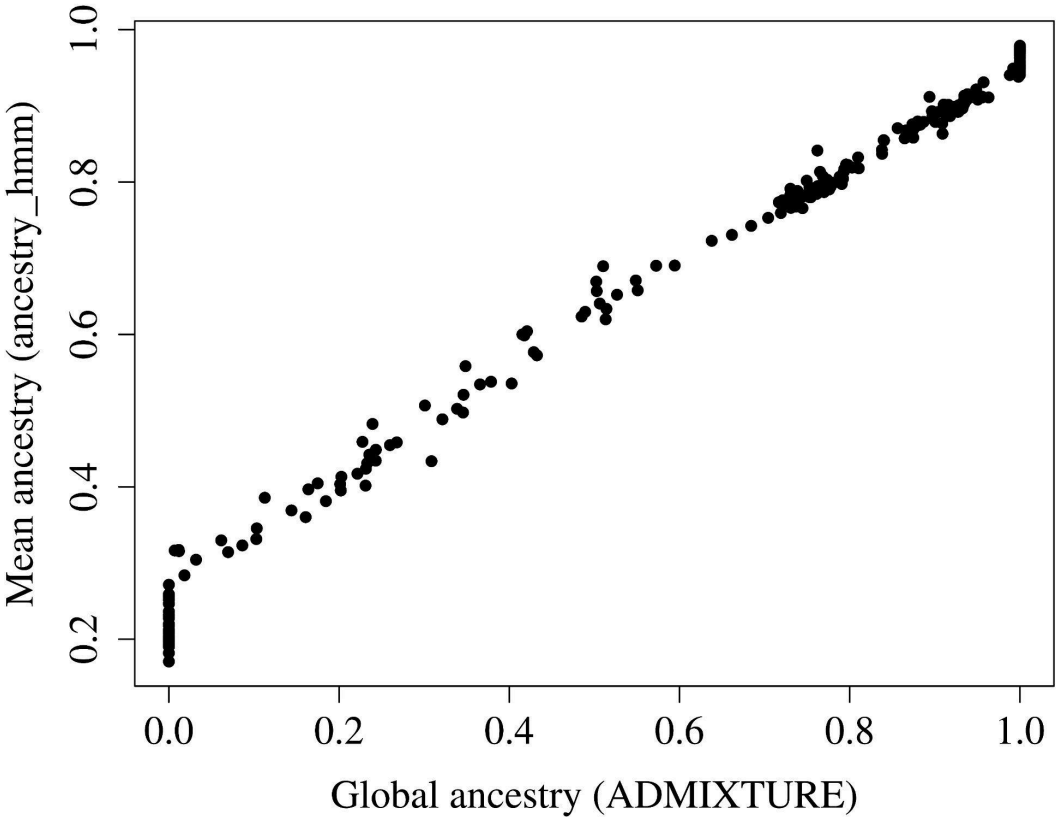

Fig. S7. Mean ancestry as calculated from the results of admixture mapping correlate to the global ancestry values resulting from ADMIXTURE analysis ($r^2 = 0.99$, p-value $< 2.2 \times 10^{-16}$).

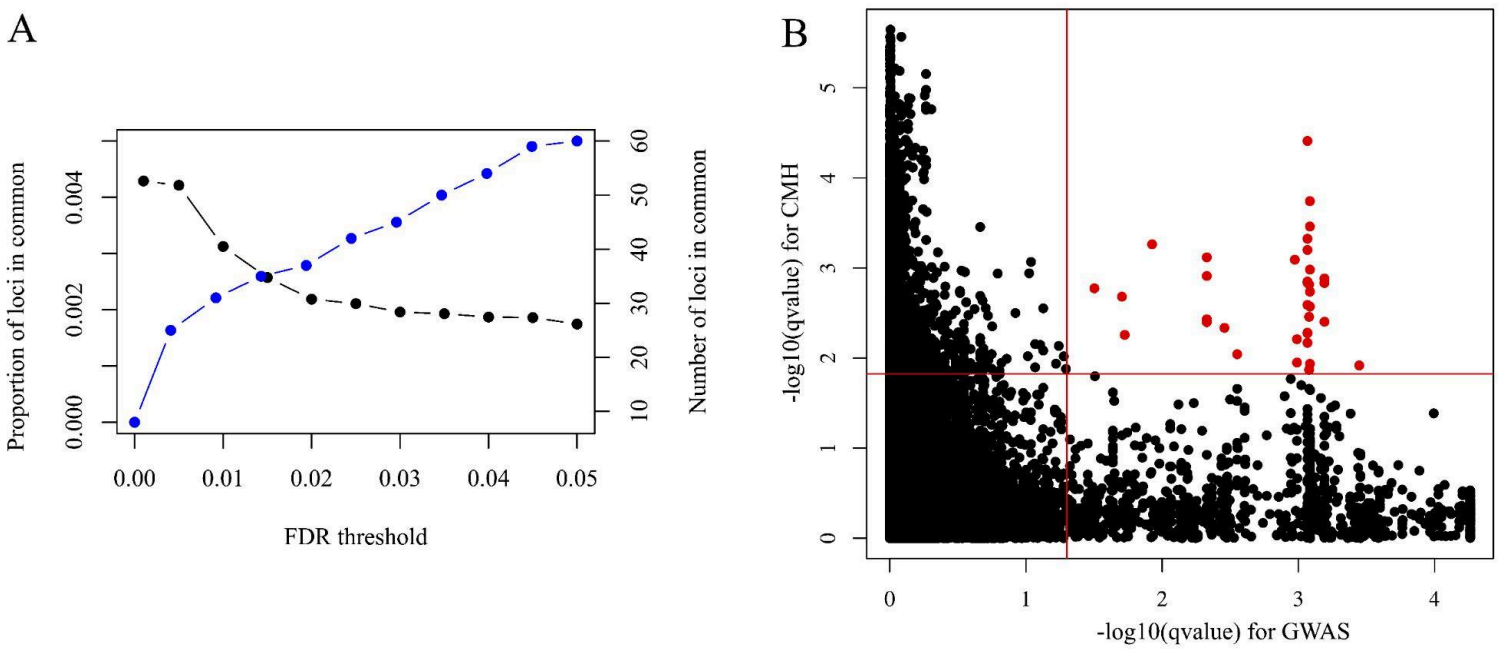

Fig. S8. (A) The number and proportion of loci in common between CMH scan and the GWAS on the drought dataset vary as a function of the FDR threshold. We chose a threshold of 0.015, which maximizes both metrics. **(B)** Common loci (black dots) and significant loci (35 loci, red dots) from the intersection between the CMH scan and the GWAS on the drought dataset. Lines denote the 0.05 (GWAS hist) and 0.015 (CMH hits) FDR threshold we used for detecting significant variants. Genes like *HAT14, RDK5*, *TBR* (all in *Arabidopsis thaliana*) and *TDC2* (*Camptotheca acuminata*) Fig. among the genes in common with both GWAS and CHM scan significant hits (see Table S1).

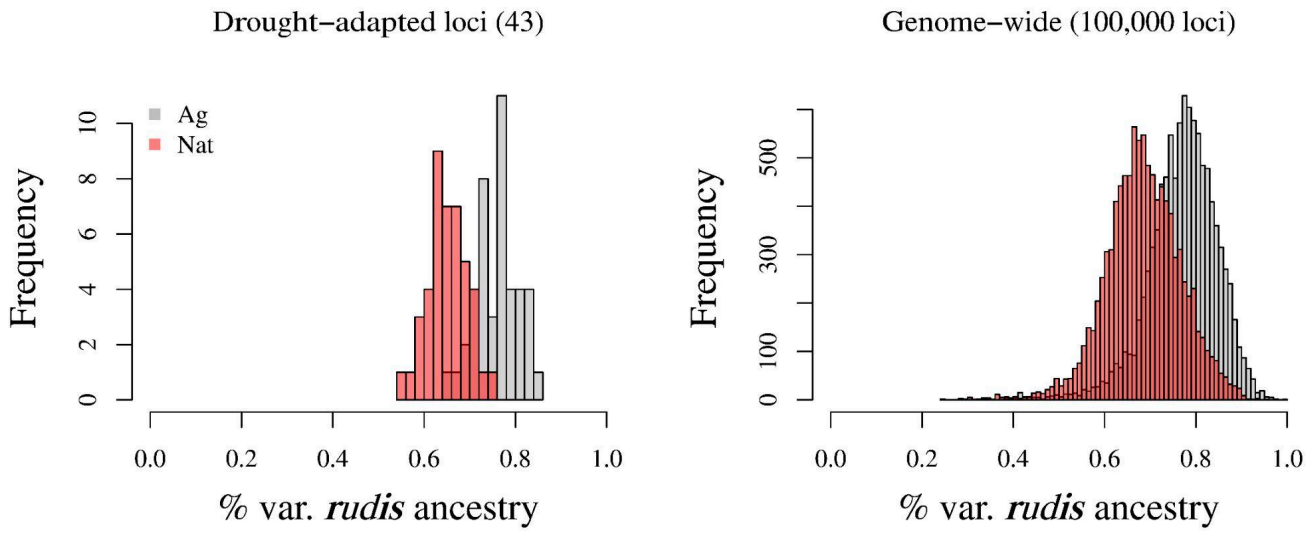

Fig. S9. Samples from agricultural habitats have significantly more var. *rudis* ancestry (mean AF = 0.76) than samples in natural habitats (mean AF = 0.65) at the 43 drought-adapted loci (Student T test t_{84}=11.332, p-value < $2x10^{-16}$). In comparison, 100,000 randomly selected loci across the genome show slightly attenuated differences in var. *rudis* ancestry across habitats (t_{19865}=77.58, p-value < $2x10^{-16}$, ag. mean AF = 0.77, and nat mean AF = 0.68).

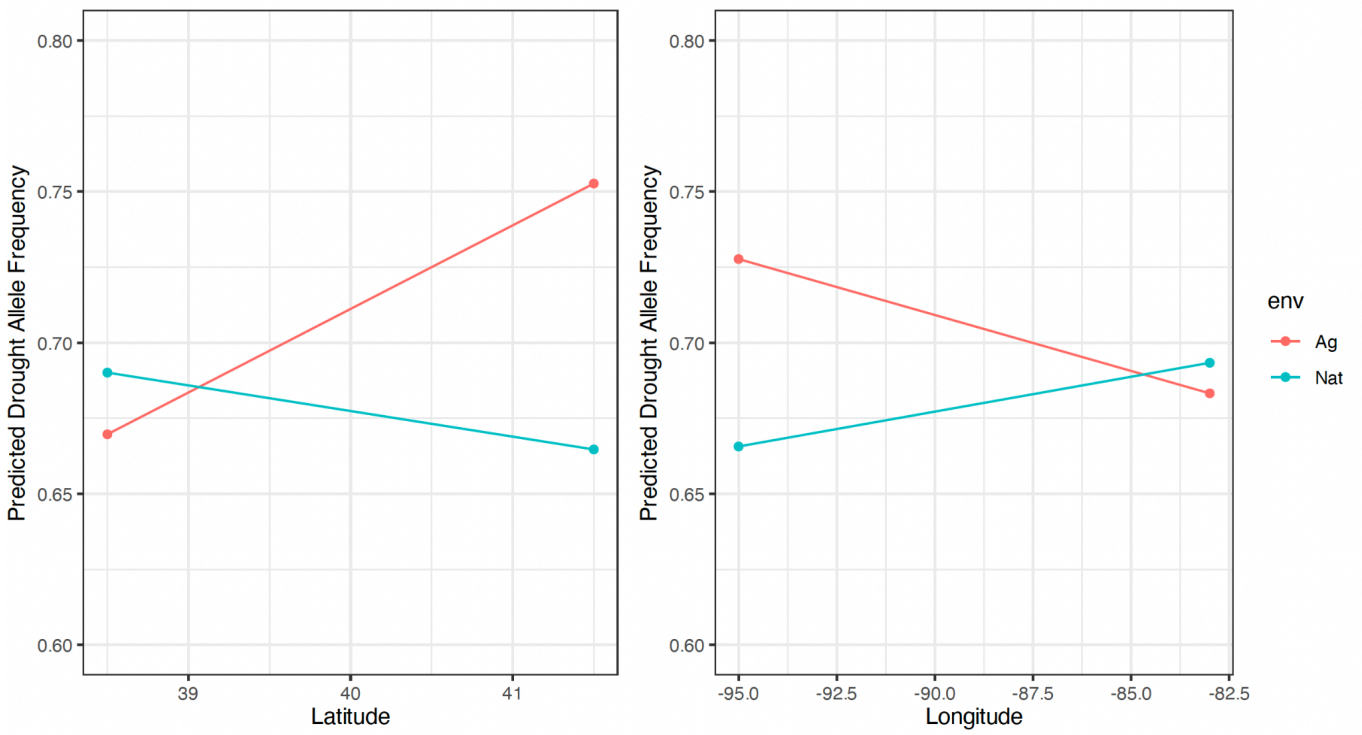

Fig. S10. The predicted effect of habitat on drought allele frequencies varies significantly with longitude and latitude, based on a multivariate linear model that controls for genome-wide ancestry.

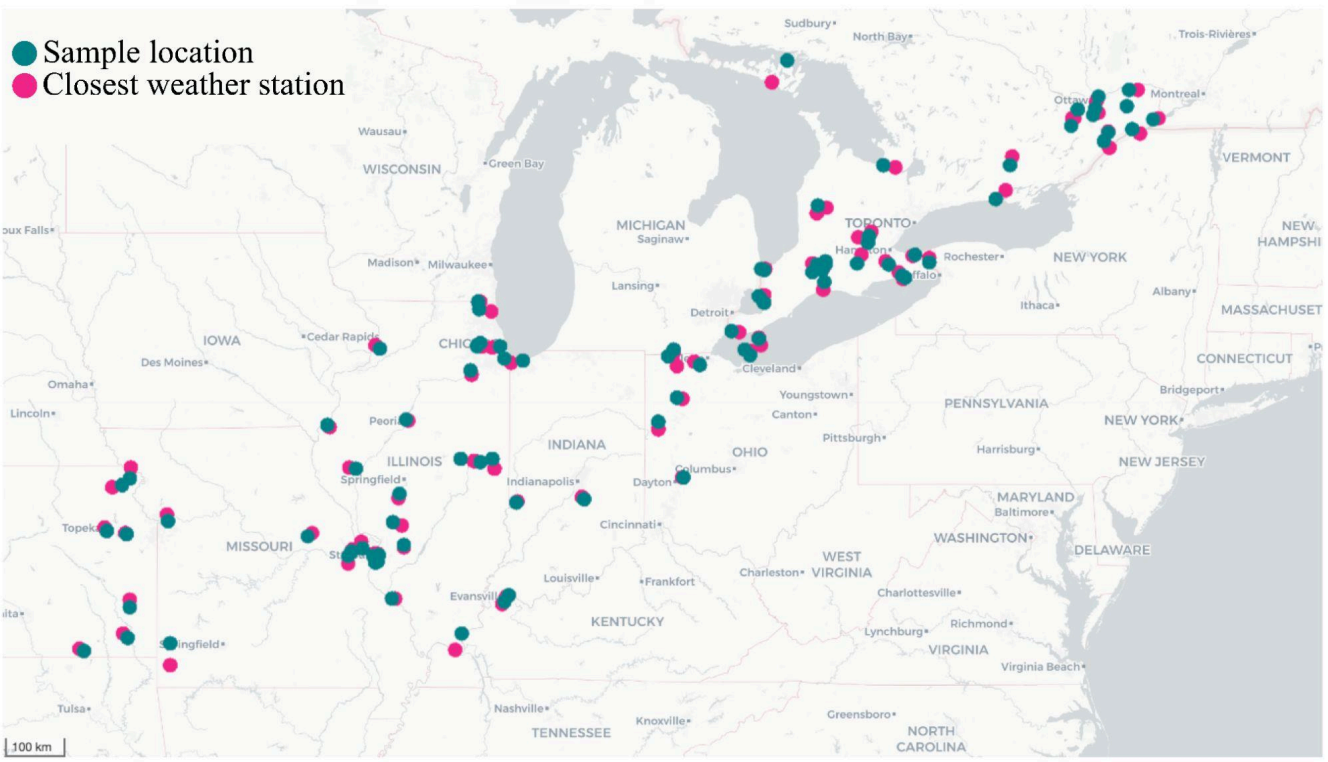

Fig. S11. Map of the herbarium samples (teal dots) and their closest weather station (pink dots, with a higher distance limit of 50 km).

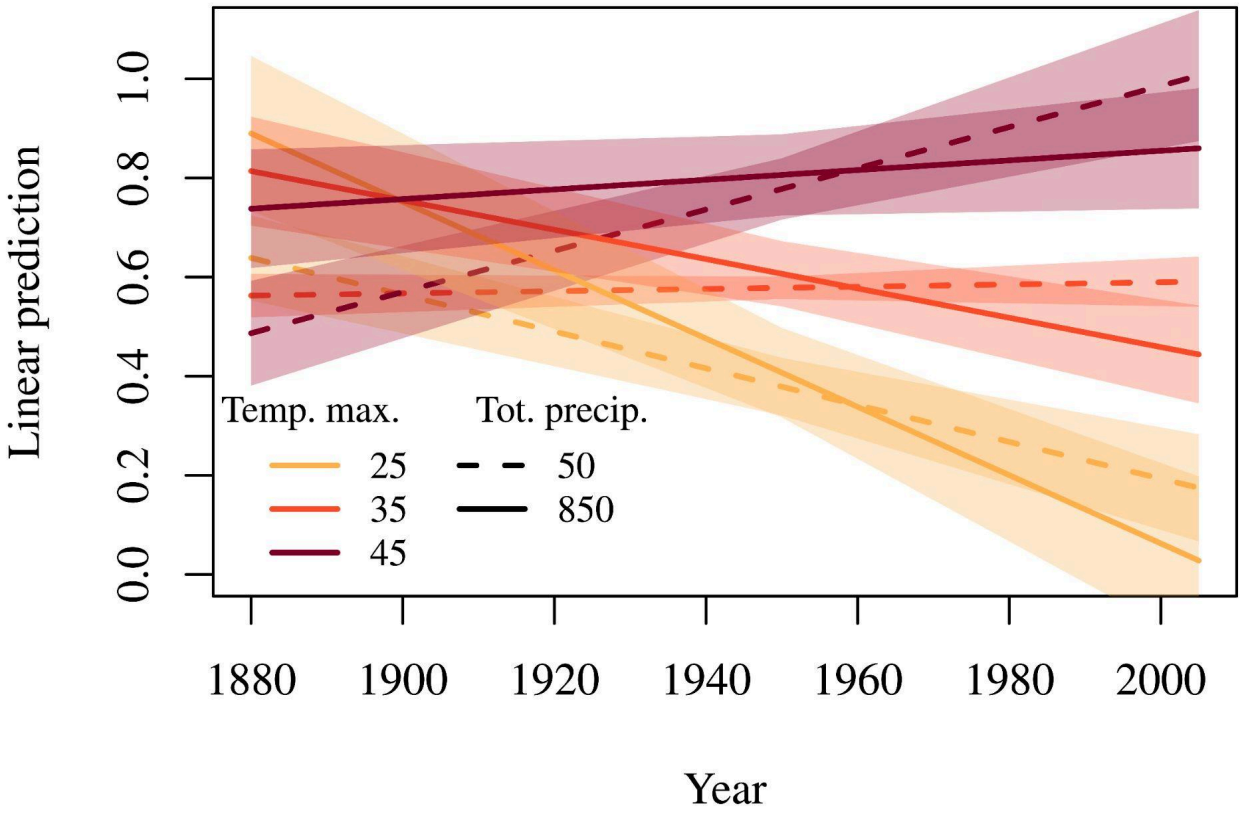

Fig. S12. When including only geographic and temporal predictors, the collective trajectory of drought loci (predicted allele frequency through time) is temperature (°C) dependent—with evidence of positive selection in hot years and negative selection in average or cool years ($F_{1,1088}$ = 8.70, p-value = 0.003 for the effect of the interaction between time and temperature, $F_{1,1088}$ = 8.41, p-value = 0.004 for the effect of temperature). The effect of precipitation (mm) on drought allele frequency trajectories is marginal ($F_{1,1088}$ = 3.03, p-value = 0.08) as is the interaction of precipitation with time ($F_{1,1088}$ = 2.98, p-value = 0.08). Predicted values inferred from a multivariate regression, also controlling for geographic variables along with sample year and climate. Model formulation : haplotype ~ tmax*year + prcp*year + locus + latitude + longitude.

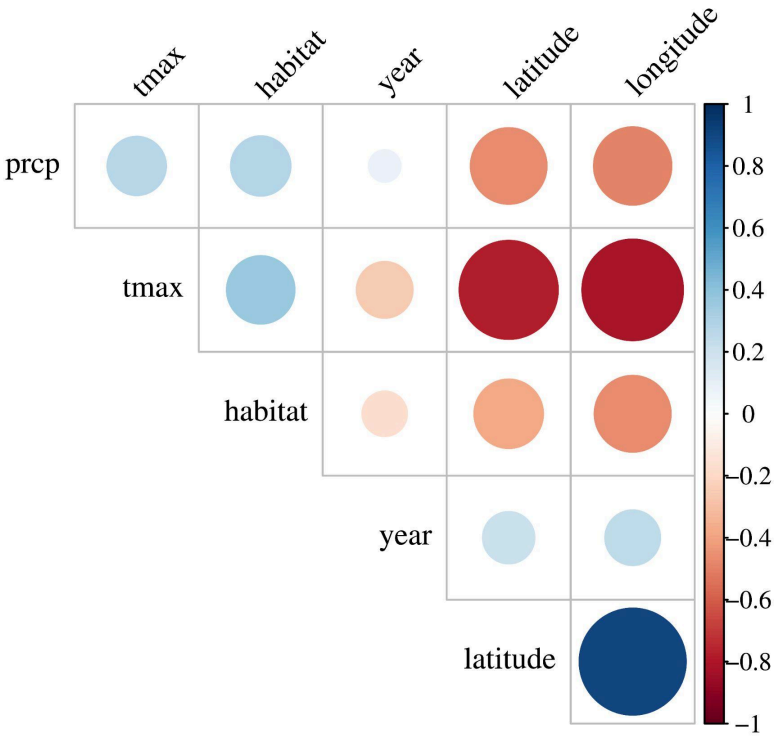

Fig. S13. Correlation matrix of the covariates from the multivariate model on haplotype change over time, space, habitat and climate (Fig. 5 analyses). All correlations were significant (Pearson's correlation test, p-value < 0.05). prcp-value = total precipitation for summer months, tmax = maximum temperature for summer months. The "habitat" covariate was turned to "1" for Agricultural and "0" for Natural habitats.

Supplementary Tables

Table S1. Response to drought depends on ancestry, regardless of ADMIXTURE or PC based metric in multivariate models. Models were implemented with two different hierarchical summaries of ancestry, at the individual and population levels.

	Ancestry	Sum Sq	Df	F	value
Population-level	(Intercept)	2.648	1	2.696	0.12011
	longitude	6.1124	1	6.2232	0.02393
	latitude	0.7919	1	0.8062	0.38255
	ADMIXTURE proportion	5.8556	1	5.9618	0.02661
	env	0.3516	1	0.358	0.55801
	longitude:ADMIXTURE proportion	7.0237	1	7.151	0.01663
	Residuals	15.715	16		
	PC1				
	(Intercept)	1.1793	1	1.2296	0.28387
	meanPC1	6.8456	1	7.1379	0.01671
	longitude	2.8544	1	2.9763	0.10375
	latitude	0.4412	1	0.46	0.50731
	env	0.4217	1	0.4398	0.51668
	meanPC1:longitude	8.0677	1	8.4122	0.01043
	Residuals	15.3446	16		
Individual-level	**Ancestry**				
	latitude	5.1	1	0.5461	4.61E-01
	longitude	5.4	1	0.578	4.48E-01
	env	11.64	1	1.2462	2.65E-01
	ADMIXTURE proportion	53.27	1	5.7049	0.01759
	longitude:ADMIXTURE proportion	42.6	1	4.5614	3.36E-02
	Residuals	2558.68	274		
	PC1				
	latitide	1.98	1	0.2116	6.46E-01
	longitude	5.2	1	0.5543	0.4572
	env	12.8	1	1.365	0.24368
	PC1	37.41	1	3.9895	4.68E-02
	longitude:PC1	48.06	1	5.1252	0.02436
	Residuals	2569.08	274		

Table S2. Variant type (as identified by snpEff) and potential functional effect of significant GWAS hits with drought tolerance.

chromosome	pos	ref	alt	type	protein_&_species
2	51130514	A	T	missense_variant	ABCA2: ABC transporter A family member 2 (Arabidopsis thaliana);
4	5060424	A	T	missense_variant	HAT14: Homeobox-leucine zipper protein HAT14 (Arabidopsis thaliana)
4	5075021	A	T	missense_variant	Similar to TBR: Protein trichome birefringence (Arabidopsis thaliana)
4	5075469	A	T	missense_variant	Similar to TBR: Protein trichome birefringence (Arabidopsis thaliana)
4	5075662	A	T	splice_region_variant&intron_variant	Note=Similar to TBR: Protein trichome birefringence (Arabidopsis thaliana);
5	37694747	A	T	missense_variant	Similar to TDC2: Tryptophan decarboxylase TDC2 (Camptotheca acuminata)
5	37694833	A	T	missense_variant	Similar to TDC2: Tryptophan decarboxylase TDC2 (Camptotheca acuminata)
5	37694869	A	T	missense_variant	Similar to TDC2: Tryptophan decarboxylase TDC2 (Camptotheca acuminata)
5	37694930	A	T	missense_variant	Similar to TDC2: Tryptophan decarboxylase TDC2 (Camptotheca acuminata)
5	37694938	A	T	missense_variant	Similar to TDC2: Tryptophan decarboxylase TDC2 (Camptotheca acuminata)
5	37695440	A	T	missense_variant	Similar to TDC2: Tryptophan decarboxylase TDC2 (Camptotheca acuminata)
5	37695515	A	T	missense_variant	Similar to TDC2: Tryptophan decarboxylase TDC2 (Camptotheca acuminata)
6	2332437	A	T	missense_variant	Protein of unknown function;
6	2332891	A	T	missense_variant	Protein of unknown function;
6	2333185	A	T	missense_variant	Protein of unknown function;
6	2396601	A	T	missense_variant	Similar to At4g34215: Probable carbohydrate esterase At4g34215 (Arabidopsis thaliana);
6	3055974	A	T	missense_variant	IPR012951 Berberine/berberine-like
6	3056020	A	T	missense_variant	IPR012951 Berberine/berberine-like
6	3458305	A	T	missense_variant	Protein of unknown function
7	6568735	A	T	missense_variant	Protein of unknown function
7	6571047	A	T	missense_variant	Protein of unknown function
7	6572134	A	T	missense_variant	Protein of unknown function
7	6572212	A	T	missense_variant	Protein of unknown function
7	6572213	A	T	missense_variant	Protein of unknown function
7	6572273	A	T	missense_variant	Protein of unknown function
7	6591276	A	T	missense_variant	Protein of unknown function
7	8207600	A	T	missense_variant	Protein of unknown function
7	8207667	A	T	missense_variant	Protein of unknown function
7	6568883	A	T	missense_variant&splice_region_variant	Protein of unknown function;
7	6572307	A	T	stop_gained	Protein of unknown function;
9	20981908	A	T	missense_variant	Similar to RKD5: Protein RKD5 (Arabidopsis thaliana);
9	20982118	A	T	missense_variant	Similar to RKD5: Protein RKD5 (Arabidopsis thaliana);
9	20981232	A	T	stop_gained	Similar to RKD5: Protein RKD5 (Arabidopsis thaliana);
9	20981616	A	T	stop_gained	Similar to RKD5: Protein RKD5 (Arabidopsis thaliana);
10	22292099	A	T	missense_variant	Similar to NOP2B: 26S rRNA (cytosine-C(5))-methyltransferase NOP2B (Arabidopsis thaliana);
10	22292115	A	T	missense_variant	Similar to NOP2B: 26S rRNA (cytosine-C(5))-methyltransferase NOP2B (Arabidopsis thaliana);
10	22292290	A	T	missense_variant	Similar to NOP2B: 26S rRNA (cytosine-C(5))-methyltransferase NOP2B (Arabidopsis thaliana);
10	22301287	A	T	stop_gained	Similar to PER17: Peroxidase 17 (Arabidopsis thaliana);
13	20668702	A	T	missense_variant	Protein of unknown function
13	20667144	A	T	missense_variant&splice_region_variant	Protein of unknown function;

13	20666046	A	T	splice_region_variant&intron_variant	Protein of unknown function;
13	20667807	A	T	splice_region_variant&intron_variant	Protein of unknown function;
16	22780805	A	T	missense_variant	Similar to APSR1: Protein ALTERED PHOSPHATE STARVATION RESPONSE 1 (Arabidopsis thaliana);
16	22781009	A	T	missense_variant	Similar to APSR1: Protein ALTERED PHOSPHATE STARVATION RESPONSE 1 (Arabidopsis thaliana);
16	22782693	A	T	missense_variant	Similar to APSR1: Protein ALTERED PHOSPHATE STARVATION RESPONSE 1 (Arabidopsis thaliana);
16	22783372	A	T	missense_variant	Similar to APSR1: Protein ALTERED PHOSPHATE STARVATION RESPONSE 1 (Arabidopsis thaliana);
16	22783480	A	T	missense_variant	Similar to APSR1: Protein ALTERED PHOSPHATE STARVATION RESPONSE 1 (Arabidopsis thaliana);
16	22784473	A	T	missense_variant	Similar to APSR1: Protein ALTERED PHOSPHATE STARVATION RESPONSE 1 (Arabidopsis thaliana);
16	22784515	A	T	missense_variant	Similar to APSR1: Protein ALTERED PHOSPHATE STARVATION RESPONSE 1 (Arabidopsis thaliana);
16	22784532	A	T	missense_variant	Atub_193_hap2_00024293-RA:cds
16	22801329	A	T	missense_variant	Similar to DDB1: DNA damage-binding protein 1 (Solanum lycopersicum);
16	22802704	A	T	missense_variant	Similar to DDB1: DNA damage-binding protein 1 (Solanum lycopersicum);
16	22808757	A	T	missense_variant	Similar to DDB1: DNA damage-binding protein 1 (Solanum lycopersicum);
16	22808916	A	T	missense_variant	Similar to DDB1: DNA damage-binding protein 1 (Solanum lycopersicum);
16	22813743	A	T	missense_variant	Similar to DDB1: DNA damage-binding protein 1 (Solanum lycopersicum);
16	22815726	A	T	missense_variant	Similar to DDB1: DNA damage-binding protein 1 (Solanum lycopersicum);
16	22820109	A	T	missense_variant	Similar to DDB1: DNA damage-binding protein 1 (Solanum lycopersicum);
16	22818417	A	T	stop_gained	Similar to DDB1: DNA damage-binding protein 1 (Solanum lycopersicum);
16	22820133	A	T	stop_gained	Similar to DDB1: DNA damage-binding protein 1 (Solanum lycopersicum);
16	22829741	A	T	missense_variant	Similar to ABCC1: ABC transporter C family member 1 (Arabidopsis thaliana);
16	22830323	A	T	missense_variant	Similar to ABCC1: ABC transporter C family member 1 (Arabidopsis thaliana);
16	22830452	A	T	missense_variant	Similar to ABCC1: ABC transporter C family member 1 (Arabidopsis thaliana);
16	22830466	A	T	missense_variant	Similar to ABCC1: ABC transporter C family member 1 (Arabidopsis thaliana);
16	22831915	A	T	missense_variant	Similar to ABCC1: ABC transporter C family member 1 (Arabidopsis thaliana);
16	22942706	A	T	missense_variant	Similar to REM4.1: Remorin 4.1 (Oryza sativa subsp. japonica);
16	22942714	A	T	missense_variant	Similar to REM4.1: Remorin 4.1 (Oryza sativa subsp. japonica);
16	22942822	A	T	missense_variant	Similar to REM4.1: Remorin 4.1 (Oryza sativa subsp. japonica);
16	22943115	A	T	missense_variant	Similar to REM4.1: Remorin 4.1 (Oryza sativa subsp. japonica);
16	22955554	A	T	missense_variant	Similar to CIPK23: CBL-interacting serine/threonine-protein kinase 23 (Arabidopsis thaliana);
16	22955666	A	T	missense_variant	Similar to CIPK23: CBL-interacting serine/threonine-protein kinase 23 (Arabidopsis thaliana);
16	22955727	A	T	missense_variant	Similar to CIPK23: CBL-interacting serine/threonine-protein kinase 23 (Arabidopsis thaliana);
16	22999020	A	T	missense_variant	Similar to TCP2: Transcription factor TCP2 (Arabidopsis thaliana);
16	22999363	A	T	missense_variant	Similar to TCP2: Transcription factor TCP2 (Arabidopsis thaliana);
16	22841981	A	T	splice_region_variant&intron_variant	Note=Similar to ABCC1: ABC transporter C family member 1 (Arabidopsis thaliana);

16	22879935	A	T	splice_region_variant&intron_variant	Protein of unknown function;
16	22941059	A	T	splice_region_variant&intron_variant	Similar to REM4.1: Remorin 4.1 (Oryza sativa subsp. japonica);
16	22939421	A	T	stop_gained	Similar to REM4.1: Remorin 4.1 (Oryza sativa subsp. japonica);
16	22955293	A	T	splice_region_variant&intron_variant	Similar to CIPK23: CBL-interacting serine/threonine-protein kinase 23 (Arabidopsis thaliana);
16	22889639	A	T	splice_region_variant&synonymous_variant	Similar to POPTRDRAFT_798217: CASP-like protein 1B2 (Populus trichocarpa);
16	22890784	A	T	stop_gained	Similar to POPTRDRAFT_798217: CASP-like protein 1B2 (Populus trichocarpa);
16	22886861	A	T	stop_gained	Protein of unknown function;

Table S3. Biological processes inferred from gene ontology analysis of 893 GWAS hits for drought-tolerance.

GO biological process complete	Arabidopsis thaliana - REFLIST	Fold Enrichment	raw P-value
mRNA 3'-end processing by stem-loop binding and cleavage (GO:0006398)	2	> 100	2.26E-03
(+)-abscisic acid D-glucopyranosyl ester transmembrane transport (GO:1902418)	2	> 100	2.26E-03
phytochromobilin biosynthetic process (GO:0010024)	3	> 100	3.38E-03
phytochromobilin metabolic process (GO:0051202)	3	> 100	3.38E-03
phenylacetate catabolic process (GO:0010124)	3	> 100	3.38E-03
glucoside transport (GO:0042946)	3	> 100	3.38E-03
xenobiotic catabolic process (GO:0042178)	4	> 100	4.51E-03
xenobiotic metabolic process (GO:0006805)	5	> 100	5.63E-03
cellular response to xenobiotic stimulus (GO:0071466)	5	> 100	5.63E-03
histone mRNA metabolic process (GO:0008334)	5	> 100	5.63E-03
glycoside transport (GO:1901656)	5	> 100	5.63E-03
xenobiotic transmembrane transport (GO:0006855)	6	> 100	6.75E-03
riboflavin biosynthetic process (GO:0009231)	8	> 100	8.99E-03
arsenite transport (GO:0015700)	8	> 100	8.99E-03
positive regulation of photomorphogenesis (GO:2000306)	8	> 100	8.99E-03
positive regulation of development, heterochronic (GO:0045962)	8	> 100	8.99E-03
potassium ion import across plasma membrane (GO:1990573)	8	> 100	8.99E-03
chloroplast-nucleus signaling pathway (GO:0010019)	9	98.48	1.01E-02
response to xenobiotic stimulus (GO:0009410)	9	98.48	1.01E-02
riboflavin metabolic process (GO:0006771)	9	98.48	1.01E-02
pollen tube reception (GO:0010483)	11	80.57	1.23E-02
flavin-containing compound biosynthetic process (GO:0042727)	12	73.86	1.35E-02
biological process involved in intraspecies interaction between organisms (GO:0051703)	14	63.31	1.57E-02
intracellular manganese ion homeostasis (GO:0030026)	14	63.31	1.57E-02
flavin-containing compound metabolic process (GO:0042726)	15	59.09	1.68E-02
mRNA 3'-end processing (GO:0031124)	15	59.09	1.68E-02
regulation of morphogenesis of a branching structure (GO:0060688)	15	59.09	1.68E-02
regulation of secondary shoot formation (GO:2000032)	15	59.09	1.68E-02
manganese ion homeostasis (GO:0055071)	16	55.39	1.79E-02
response to nutrient (GO:0007584)	16	55.39	1.79E-02
regulation of plant organ formation (GO:1905428)	19	46.65	2.12E-02
response to arsenic-containing substance (GO:0046685)	19	46.65	2.12E-02
rRNA base methylation (GO:0070475)	19	46.65	2.12E-02
inorganic cation import across plasma membrane (GO:0098659)	19	46.65	2.12E-02
inorganic ion import across plasma membrane (GO:0099587)	20	44.31	2.23E-02
root hair initiation (GO:0048766)	20	44.31	2.23E-02
snRNA processing (GO:0016180)	21	42.2	2.34E-02
chloroplast accumulation movement (GO:0009904)	21	42.2	2.34E-02
potassium ion transport (GO:0006813)	51	34.76	1.52E-03
snRNA metabolic process (GO:0016073)	27	32.83	3.00E-02
dicarboxylic acid biosynthetic process (GO:0043650)	28	31.65	3.11E-02
xenobiotic transport (GO:0042908)	57	31.1	1.89E-03
rRNA methylation (GO:0031167)	29	30.56	3.22E-02
establishment of plastid localization (GO:0051667)	29	30.56	3.22E-02
chloroplast relocation (GO:0009902)	29	30.56	3.22E-02
import across plasma membrane (GO:0098739)	33	26.86	3.66E-02
potassium ion transmembrane transport (GO:0071805)	34	26.07	3.77E-02
chloroplast localization (GO:0019750)	34	26.07	3.77E-02
maturation of LSU-rRNA (GO:0000470)	34	26.07	3.77E-02
plastid localization (GO:0051644)	35	25.32	3.88E-02

fatty acid beta-oxidation (GO:0006635)	36	24.62	3.99E-02
positive gravitropism (GO:0009958)	36	24.62	3.99E-02
regulation of photomorphogenesis (GO:0010099)	40	22.16	4.42E-02
fatty acid oxidation (GO:0019395)	40	22.16	4.42E-02
lignin biosynthetic process (GO:0009809)	41	21.62	4.53E-02
rRNA modification (GO:0000154)	43	20.61	4.74E-02
fatty acid catabolic process (GO:0009062)	43	20.61	4.74E-02
inorganic cation transmembrane transport (GO:0098662)	204	8.69	2.21E-02
metal ion transport (GO:0030001)	227	7.81	2.70E-02
monoatomic cation homeostasis (GO:0055080)	242	7.32	3.04E-02
inorganic ion transmembrane transport (GO:0098660)	256	6.92	3.37E-02
monoatomic ion homeostasis (GO:0050801)	260	6.82	3.46E-02
monoatomic cation transport (GO:0006812)	264	6.71	3.56E-02
monoatomic ion transport (GO:0006811)	293	6.05	4.30E-02
phosphorylation (GO:0016310)	528	5.04	2.13E-02
establishment of localization (GO:0051234)	2263	3.13	2.95E-03
localization (GO:0051179)	2434	2.91	4.63E-03
transport (GO:0006810)	2137	2.9	8.52E-03

Table S4. ANOVA results from multivariate logistic and linear models of joint allele frequency change of all drought loci across sequenced herbarium samples spanning spatiotemporal scales, before and after accounting for collection habitat (classified as disturbed, agricultural, or natural) and its interaction with time.

	Linear model	Sums of Squares	DF	F	p-value
No habitat	(Intercept)	0.935	1	7.4246	0.0065371
	tmax	1.059	1	8.4072	0.0038124
	year	1.126	1	8.941	0.0028512
	prcp	0.381	1	3.0282	0.0821114
	locus	6.421	32	1.5935	0.0198677
	samp_lat	1.745	1	13.8551	0.0002076
	samp_lon	0.496	1	3.9362	0.0475087
	tmax:year	1.096	1	8.7026	0.0032455
	year:prcp	0.375	1	2.9817	0.0844971
	Residuals	136.996	1088		
With habitat	Linear model	Sums of Squares	DF	F	p-value
	(Intercept)	0.187	1	1.5924	0.207276
	tmax	0.06	1	0.5108	0.474952
	year	0.108	1	0.9221	0.337161
	prcp	0.526	1	4.4895	0.034349
	env	0.697	2	2.9705	0.05173
	locus	5.524	32	1.4721	0.044934
	latitude	3.532	1	30.1238	0.0000000514
	longitude	0.952	1	8.1198	0.004468
	tmax:year	0.046	1	0.3964	0.529084
	year:prcp	0.51	1	4.3487	0.037289
	year:env	0.7	2	2.9838	0.05105
	Residuals	117.488	1002		

	Logistic model	Chisq	DF	p-value
No habitat	tmax	4.5502	1	0.032915
	year	4.8359	1	0.027872
	prcp	1.6811	1	0.194773
	locus	27.236	32	0.706567

	latitude	7.5157	1	0.006116
	longitude	2.0563	1	0.151575
	tmax:year	4.7095	1	0.029996
	year:prcp	1.6545	1	0.198346
With habitat	Logistic model	Chisq	DF	p-value
	tmax	0.2481	1	0.61843
	year	0.4621	1	0.49664
	prcp	2.4166	1	0.12006
	locus	23.3951	32	0.86547
	latitude	15.277	1	9.28E-05
	longitude	4.1616	1	0.04135
	env	2.9956	2	0.22363
	tmax:year	0.1915	1	0.6617
	year:prcp	2.3425	1	0.12589
	year:env	3.0081	2	0.22223